DIPLOMARBEIT

Implementation of IEEE 802.11p Physical Layer Model in SIMULINK

ausgeführt zum Zwecke der Erlangung des akademischen Grades
einer Diplom-Ingenieurin

unter der Leitung von
Univ.Prof. Dipl.-Ing. Dr.techn. Christoph F. Mecklenbräuker
Univ.Ass. Dipl.-Ing. Alexander Paier
Institut für Nachrichtentechnik und Hochfrequenztechnik

eingereicht an der Technischen Universität Wien
Fakultät für Elektrotechnik und Informationstechnik

von
Veronika Shivaldova
Landstraßer Gürtel 21/14
1030 Wien

Wien, im Juni 2010 _____

Посвящается
светлой памяти моей любимой бабушки
Шивалдовой Натальи Петровны

Abstract

The dramatic increase of road traffic raises demand for co-operative systems that improve safety and efficiency in transport. Road safety is potentially enhanced by the deployment of wireless communication technologies for vehicular networks, which enable new services such as collision detection and avoidance, traffic management and adaptive control. Aiming at reliable wireless connectivity for vehicular networks, the IEEE 802.11p standard specifies a physical layer transmission format and a medium access control protocol for vehicular applications worldwide. Currently, the research community is analyzing the IEEE 802.11p link-layer performance through the use of simulation tools and experiments on the road. In spite of the increased academic and industrial efforts, the standard's dependability in high-mobility scenarios remains a major challenge.

This thesis presents an implementation of a complete Orthogonal Frequency Division Multiplexing (OFDM) physical layer in Matlab SIMULINK, designed according to the specification in the draft amendment IEEE 802.11p version D9.0. After a brief introduction to vehicular communications together with the ongoing standardization activities and the promising applications, I describe the implementation of the transceiver and outline the methodology that was used during the development process. In order to investigate the performance and reliability of the physical layer, several realistic propagation channel models, as well as one reference channel model are employed. Finally, design parameters and useful optional extensions for the receiver that are crucial for performance optimization of vehicular communication systems are analyzed. Performance gains achieved with extended receiver design (soft demapping and decoding, smoothing of the estimated channel coefficients), as well as influence of propagation channel parameters on the overall system behavior are demonstrated based on numerical simulation results.

Zusammenfassung

Durch die dramatische Zunahme des Verkehrsaufkommens steigt die Nachfrage nach kooperativen Systemen, die die Sicherheit und Effizienz von Transport-Systemen verbessern können. Die Verkehrssicherheit kann durch den Einsatz von drahtlosen Fahrzeug-Kommunikations-Technologien wesentlich erhöht werden. Diese Technologien ermöglichen neue Dienste, wie beispielsweise Kollisionserkennung und Kollisionsverhinderung, Verkehrsregelung und adaptiven Verkehrssteuerung. Um die zuverlässige, drahtlose Fahrzeug-Kommunikation zu verwirklichen spezifiziert der Standard IEEE 802.11p Übertragungsformat der physikalischen Schicht und Media Access Control Protokol für Fahrzeugkommunikationen weltweit. Die Forschungsgemeinschaft hat bereits begonnen, die Leistungfähigkeit der IEEE 802.11p Verbindungsschicht anhand von Simulationen und realen Messungen zu analysieren. Trotzdem bleibt die Auswertung der Robustheit des Standards unter der Anwendung von Ausbreitungsszenarien bei höheren Geschwindigkeiten eine große Herausforderung.

Diese Diplomarbeit präsentiert eine Implementierung der physikalischen Schicht, basierend auf OFDM, in Matlab SIMULINK, entworfen gemäß der Spezifizierung in IEEE 802.11p Version D9.0. Nach einer kurzen Einleitung in die Fahrzeug-Kommunikation zusammen mit der Beschreibung von laufenden Standardisierungstätigkeiten und Anwendungen, beschreibe ich die Struktur des Sendeempfängers und stelle die Methodik, die während des Entwicklungsprozesses verwendet wurde, dar. Um die Leistungsfähigkeit und Zuverlässigkeit der physikalischen Schicht zu untersuchen, wurden mehrere realistische Kanalmodelle, sowie ein Referenzkanalmodell verwendet. Schließlich werden die Entwurfsparameter und einige optionale Erweiterungen für den Empfänger, die für die Optimierung der Leistungsfähigkeit von Fahrzeug-Kommunikationssystemen entscheidend sind, analysiert. Gewinne hinsichtlich der Leistungsfähigkeit, die mit dem erweiterten Empfänger-Design erreicht werden können, sowie der Einfluss von verschiedenen Ausbreitungskanälen auf das gesamte Systemverhalten, werden anhand von numerischen Simulierungsergebnissen demonstriert.

Acknowledgements

First and foremost I would like to express my sincerest gratitude to Prof. Christoph Mecklenbräuker for suggesting the topic of this thesis and guiding my analysis. Further I highly appreciate the opportunity to present the results of my work at the regular meetings of the research module for Vehicular Connectivity within the Christian Doppler Laboratory for Wireless Technologies for Sustainable Mobility. Constant interest in my research progress and fruitful discussions have fuelled much motivation for this thesis.

I would also like to gratefully acknowledge the enthusiastic supervision of Alexander Paier, who has supported me with patient guidance, great kindness and friendly assistance during the preparation and completion of this project. His careful proofreading, accomplished in different parts of the world, improved both the presentation and the quality of this work significantly.

I am particularly indebted to the Mondi Austria Private Foundation for financing of my studies and providing me with the great opportunity to grow as a student and engineer in the unique research environment of the Vienna University of Technology.

Special thanks goes to Sabine Cirtek, coordinating the "fForte WIT - Women in Technology" project, for offering me the opportunity to participate in numerous seminars, workshops and training programs that have considerably contributed to my personal and professional development.

I greatly appreciate the overall support and care of Barbara and Helmut, who have been a constant source of warm feelings and have strengthened me with their familiar and friendly spirit.

Over all this I am indebted to my best friend, companion and the love of my life, Andreas, who only knows the real price of this thesis, as we have paid it together. His endless patience, understanding, love and encouragement have inspired me all over again whenever my endurance and ambition were approaching their lower bounds. Without him accomplishing the studies and this thesis would never be possible indeed.

Больше всех я благодарна своим родителям и бабушке за их безграничную любовь, заботу и понимание, которые являлись постоянным источником вдохновения и значимой составляющей моего успеха. Безусловно, я бы не смогла преодолеть и сотой доли моего пути, если бы не ваша вера в меня и гордость за мои успехи. Спасибо, что вы сделали возможным моё образование, что были рядом каждой частичкой своей души и преодолевая границы пространства и времени радовались моим победам и смягчали мне горесть поражений.

Contents

1

Introduction

Over the past few years vehicular communications have gained wide popularity and importance in both academia and industry. This technology offers broad range of applications including public safety, vehicular traffic coordination, road traffic management, and comfort applications [1]. However, most of research projects aim their attention at public safety applications, which promise to decrease the number of accidents and save human lives. Unfortunately, the penetration of this scientific know-how is still weak and much research remains to be done, to bring alive the vision of future Intelligent Transport Systems (ITS). This thesis presents a standardized transmission model, that intends to cope with some challenging characteristics of vehicular communication and investigates the model's behavior in various transmission scenarios.

1.1 Applications and Services

As mentioned above, the most promising applications of inter-vehicle communication are public safety applications, which are geared primarily toward avoiding accidents and loss of human life. Public safety applications can be divided in two classes: Cooperative Collision Avoidance (CCA) and Emergency Warning Message (EWM) [1]. In case of CCA vehicles either identify potential collision situation and inform the driver, or warn the driver about already occurred collision, in order to avoid other vehicles from driving into crash. A multilane highway during rush hour is considered as one of scenarios with high risks of collisions due to lane change, this particular case involves that thousands vehicles need to be informed and coordinated simultaneously in very short time. On a single-lane road only few vehicles are involved and the major risk factor turns to be a head-on collision that imposes very high relatively speed of vehicles. The major characteristic for CCA applications is high demand on the latency and reliability. Moreover, as it was shown in the example above, in case of dense highway and high speed, radio propagation conditions will become the great challenge.

The other important type of public safety related application is the EWM. In this case vehicles spread out not only accident related information, but also hazardous road condition warnings. Depending on matter of warning message, one should distinguish between instant EWM applications, which are relevant only for a limited time period and abiding EWM applications, which aim to warn drivers in the zone of relevance during a long time period [2]. In case, a vehicle is rapidly decreasing speed, EWM application will send an instant emergency message, warning drivers in relevant area about possible collision. However, this information becomes irrelevant after some time and thus will “disappear”. In contrast to instant EWM, emergency messages warning drivers about hazardous road conditions, such as snow, ice, slippery road or obstacles in the way, needs to stay in relevant area over a longer time, so that any vehicle entering the area is able to access this information. It is quite challenging to ensure reliable EWM dissemination on roads with low traffic (i.e., during the night) on Vehicle-to-Vehicle (V2V) manner. Therefore, a solution assuming some infrastructure (Vehicle-to-Infrastructure (V2I) and Infrastructure-to-Vehicle (I2V)) was proposed.

In contrast to public safety related applications, traffic coordination and management applications have less strict demand on latency and reliability. This category of applications aims to assist drivers by giving them essential tools to decide the best route along the way. In particular vehicular traffic coordination applications attempt to reduce or eliminate risks of such maneuvers, like lane change or passing on multilane highway with heavy traffic. Road traffic management applications are focused on improving traffic flow, thus reducing both congestions and travel times. Considerable impact on congestion avoidance have traffic monitoring applications, that can provide high-resolution, localized traffic information, e.g.,

speed, and in-place traffic view for several miles around the current location of the vehicle. This information will improve the performance of the vehicle's navigation system and will speed up the traffic flow.

Apart of the safety and traffic management applications, vehicular networks can be exploited to enable entertainment and comfort applications for drivers (e.g., local information regarding restaurants and hotels) and for passengers (e.g., internet or in-vehicle TV). The driving forces in development of this application class have been network operators, service providers, and number of industrial and telecom companies that can see business advantages when providing this application to the market.

1.2 Frequency Band Allocation

Pioneer in frequency band allocation for vehicular communications was the U.S. Federal Communication Commission that has allocated 75 MHz spectrum at 5.9 GHz exclusively for V2V and I2V communications in North America. Process of frequency allocation in Europe is considerably more complex, since all European countries and their authorities are involved. In August 2008, after spectrum requirements have been analyzed and frequency regulation and redeployment have been worked out, the Commission of European Communities has carried out the decision on the harmonized use of radio spectrum in the $5875 - 5905$ MHz frequency band for safety related applications of ITS [3].

The primary purpose of this frequency band allocation was to enable reliable and fast real-time communication between vehicles and road, in order to reduce number of accidence, avoid potentially dangerous traffic situations and improve user mobility comfort. European Conference of Postal and Telecommunications Administrations (CEPT) concluded in its report [4] that ITS safety-related applications in the frequency range $5875 - 5905$ MHz are compatible with all other services in this frequency band. Moreover, the whole 75 MHz band in range $5850 - 5925$ MHz may be used for ITS applications in future, as long as they comply with certain emission limits. Thus the frequency band allocated for safety-related ITS applications in Europe conforms to spectrum used in other regions and in this manner contributes for global harmonization.

According to nominal carrier frequency allocation, defined by European Telecommunications Standards Institute (ETSI) in its Harmonized Standard EN 302 571 [5], the whole 75 MHz frequency band is divided in seven channels, each of which is 10 MHz wide. As shown in Figure 1.1, the fourth channel is preserved for system control, whereas the other six channels are used for services. Control channel is utilized for transmission of high priority messages and management information. Channels one and two are intended for non-safety

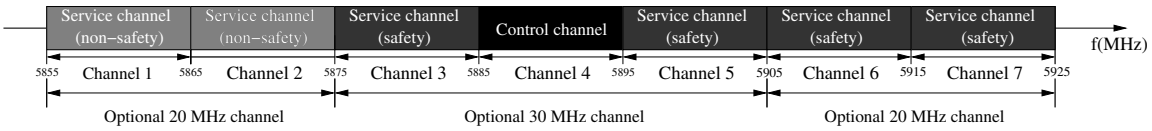

Figure 1.1: *Nominal carrier frequency allocation for WAVE.*

applications and the rest is utilized by safety services. It is important to note that throughput of each 10 MHz channel can vary from 3 to 27 Mb/s, depending on the used modulation scheme. In order to obtain higher throughput (up to 54 Mb/s) first and second channels, as well as sixth and seventh channels can be optionally combined to form a 20 MHz channel. Moreover, channels three, four and five can also be merged to achieve overall channel bandwidth of 30 MHz and thus further increase data rate.

1.3 IEEE Standards for Wireless Access in Vehicular Environments

Besides allocation of protected frequency band for road safety applications in Europe, definition of ubiquitous communication mechanisms between vehicles is an important issue. The IEEE 1609 Family of Standards for WAVE:11p+1609 completely address this issue, and defines a communication architecture and a standardized set of interfaces that collectively enable secure V2V and V2I wireless communications. The objective of communication architecture is to provide communication facilities for a wide range of applications. Communication architectures are usually based on the layered Open Systems Interconnection (OSI)-model, where each level provides certain functions. The Wireless Access in Vehicular Environments (WAVE) communication architecture optimized for the vehicular environment underlining involved standards is shown in Figure 1.2 and described below.

WAVE upper layers support functions required by applications, such as data transfer, resource management, system configuration, and notification. In particular, the services and interfaces of the WAVE Resource Manager application are specified in standard IEEE 1609.1 [6]. It defines numerous message formats (i.e., command, status and request) and the appropriate responses to those messages, as well as data storage formats that must be used by applications to communicate between architecture components. Networking Services, defined in IEEE 1609.3 [7] standard, consist of data and management components. Data plane components include Logical Link Control (LLC), User Datagram Protocol (UDP) and Transmission Control Protocol (TCP), as well as WAVE Short Messages Protocol (WSMP). Management services cover application registration, as well as monitoring of channel usage and received channel power indicator.

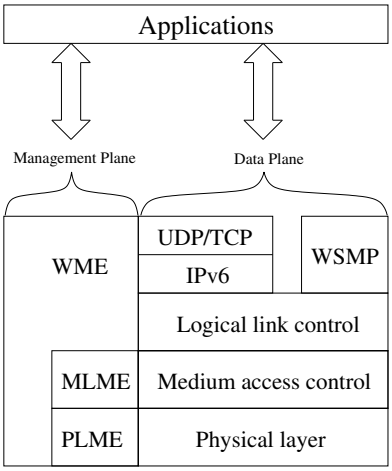

Figure 1.2: *WAVE protocol stack.*

Objective of security services is to provide authentication of control information. These services are outlined in standard IEEE 1609.2 [8], where secure message formats and its processing are determined. Furthermore, this standard summarizes circumstances under which secure messages should be used and explains how those messages should be processed.

Medium Access Control (MAC) layer and PHY are denoted as lower layers. They are specified in modified version of the IEEE 802.11a standard, known as IEEE 802.11p [9]. Since the original IEEE 802.11a standard was optimized for local area networks with no or low mobility, it could barely handle fast fading conditions, resulting from very high user mobility in vehicular networks. Amendments defined in IEEE 802.11p aims to ensure interoperability between wireless devices that interact in rapidly changing communication environments and handle situations where transactions must be completed in a time-frame, much shorter than that of IEEE 802.11a. MAC layer enables participants of vehicular network to establish a network or join a pre-existing network and to transmit data passed down by LLC. Beyond the standard functionality usually performed by MAC layers, the IEEE 802.11 MAC performs other functions that are typically related to upper layer protocols, such as fragmentation, packet retransmissions, and acknowledgements. Further consideration of MAC Layer is out of scope of this thesis and can be found in [10]. An overview of PHY, as well as major differences between IEEE 802.11a and IEEE 802.11p can be found in Subchapter 1.4.

1.4 Overview of PHY and Differences between IEEE 802.11p and IEEE 802.11a

PHY defined in standard IEEE 802.11 consists of Physical Medium Dependent (PMD) sublayer and Physical Layer Convergence Protocol (PLCP) sublayer. The PMD sublayer specifies signal build up parameters, such as modulation and channel coding and convert signal into analog form with regard to specific PHY type[1]. PLCP deals with differences among various PHYs and ensures that the MAC layers receive packets of common format, independently of particular PMD sublayer.

Convergence procedure performed by PLCP sublayer converts the actual data frame being sent, named PLCP Service Data Unit (PSDU) into PLCP Protocol Data Unit (PPDU). In terms of this convergence the PSDU is appended with preamble and header. The PLCP preamble is composed out of ten repetitions of short training sequence and two repetitions of a long training sequence, preceded by Guard Interval (GI). PLCP header contains information about transmission rate and number of octets in the PSDU, as well as tail and pad bits. PSDU itself is prepended with SERVICE field and appended with tail and pad bits to form the DATA field of PPDU frame.

For transmission an OFDM technique with 64 subcarriers is used. To design easy-to-implement transmission system, 64 carriers are defined, but only the inner 52 carriers are utilized. Out of 52 carriers 48 contains the actual data and 4 subcarriers, called pilot subcarriers, transmit a fixed pattern, used to disregard frequency and phase offset at the receiver side. Each of 48 data subcarriers can be modulated with BPSK, QPSK, 16QAM or 64QAM. In combination with different coding rates, this leads to a nominal data rate of 6 to 54 Mb/s if full clocked mode with 20 MHz bandwidth is used. IEEE 802.11p uses the half clocked mode with 10 MHz bandwidth, in order to make signal more robust against fading, resulting in corresponding data rate reduction. Some other differences between IEEE 802.11a and IEEE 802.11p due to reduced sampling rate are emphasized in Table 1.1.

In this work IEEE 802.11p standard consistent PHY model is simulated with Matlab SIMULINK to investigate model's behavior in various propagation scenarios. Thesis is organized in six chapters and gives detailed overview of all standard defined system elements, as well as implementational aspects and theoretical background. Chapter 2 describes transmitter side, where intended for transmission binary sequence is modulated and conformed into OFDM symbols. OFDM data symbols are than prepended with preamble and header to

[1]The original IEEE 802.11 defines three PHYs, two based on 2.4 GHz Industrial, Scientific and Medical (ISM) band and one based on diffused infra-red radiation, with rate up to 2 Mb/s. Later extensions define three further PHYs: IEEE 802.11a using 5 GHz spectrum for maximum channel rate of 54 Mb/s, IEEE 802.11b using 2.4 GHz spectrum for maximum channel rate of 11 Mb/s, IEEE 802.11g using 2.4 GHz spectrum for maximum channel rate of 54 Mb/s.

Parameters	**IEEE 802.11a**	**IEEE 802.11p**	**Changes**
Bit rate (Mb/s)	$6, 9, 12, 18, 24,$ $36, 48, 54$	$3, 4.5, 6, 9, 12,$ $18, 24, 27$	Half
Modulation mode	BPSK, QPSK, 16QAM, 64QAM	BPSK, QPSK, 16QAM, 64QAM	No change
Code rate	$1/2, 2/3, 3/4$	$1/2, 2/3, 3/4$	No change
Number of subcarriers	52	52	No change
Symbol duration	$4\,\mu$s	$8\,\mu$s	Double
Guard time	$0.8\,\mu$s	$1.6\,\mu$s	Double
FFT period	$3.2\,\mu$s	$6.4\,\mu$s	Double
Preamble duration	$16\,\mu$s	$32\,\mu$s	Double
Subcarrier spacing	$0.3125\,$MHz	$0.15625\,$MHz	Half

Table 1.1: *Comparison of PHYs implementations in IEEE 802.11a and IEEE 802.11p*

form a frame that is subsequently transmitted over the channel, discussed in Chapter 3. At the receiver side, outlined in Chapter 4, signal corrupted by the channel is demodulated and decoded to obtain received binary sequence. To disregard distortion effects introduced by multipath propagation and high relative velocity channel estimation and equalization are accomplished. Model performance is highly dependent on the effects introduced by the channel and techniques to compensate for these effects performed by the receiver. These dependencies are summarized and discussed in Chapter 5, which furthermore compares simulation results with real measurements in terms of Frame Error Ratio (FER). Finally concluding remarks and outlook are summed up in the last chapter.

2

Transmitter

This chapter covers all intermediate steps, performed on binary data, in order to prepare it for wireless transmission over a channel. Each step of this convergence procedure corresponds to a certain simulator block and is depicted in Figure 2.1.

First of all the binary sequence from the source block, corresponding to PSDU, is encoded and modulated. The encoding process is composed of scrambling, encoding, interleaving and possibly puncturing, in order to achieve higher data rates. The resulting coded and interleaved data string is converted into a complex number according to certain signal constellation and subsequently divided into groups of 48 complex numbers and mapped to OFDM subcarriers. In the assembler block 4 pilot subcarriers and 1 zero DC subcarrier are inserted among 48 data subcarriers, which are then wrapped in 11 zero guard subcarriers to form an OFDM symbol. The next block converts the subcarriers to time domain using Inverse Fast Fourier Transformation (IFFT) and prepends time domain signal with circular extension of itself to form cyclic prefix. In the last stage of the transmitter, OFDM data symbols are appended one after another and provided with a PLCP preamble and header to create a complete PPDU frame, which is now ready for transmission over a channel.

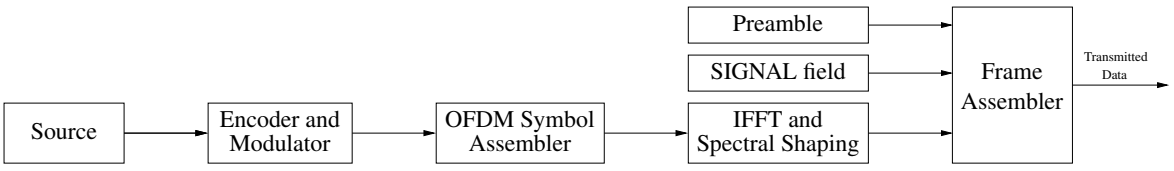

Figure 2.1: *Block diagram of the transmitter.*

Fundamentals of OFDM theory that are crucial for understanding of the implemented transmission model are briefly described in subchapter 2.1.

2.1 OFDM Theory

OFDM is a multicarrier transmission technique that divides the available band into K subbands, corresponding to subcarriers with frequency separation F. Subcarriers are modulated by low-rate data streams that are achieved by splitting the high-rate stream into K parallel substreams. From this perspective OFDM is similar to Frequency Division Multiple Access (FDMA). However, in FDMA all subcarriers are spectrally disjoint and require spectral guard intervals in order to prevent interference between closely spaced subcarriers. OFDM uses the spectrum much more efficiently by spacing subcarriers closer together and preventing interference by making all the carriers orthogonal to one another. Orthogonality of the carriers means that an integer multiple of cycles is contained in each symbol interval. Thus the spectrum of each carrier has a null at the centre frequency of each of the other carriers and carriers can be spaced as close as theoretically possible without interference. This overcomes problems of overhead carrier spacing and guard interval allocation required in FDMA [11].

Assume that we have K orthogonal basis functions or pulse shapes $g_k(t)$, with $k = 0, 1, \ldots K-1$. In the n-th symbol interval K symbols $a_k[n]$ from a certain symbol alphabet are transmitted simultaneously. These symbols are amplitude factors of K orthogonal pulses $g_k(t - nT_s)$. Thus the transmit signal component corresponding to the n^{th} symbol interval is

$$s_n(t) = \sum_{k=0}^{K-1} a_k[n] g_k(t - nT_s) e^{j2\pi kFt}. \tag{2.1}$$

The signal components corresponding to various symbol intervals are added to yield the overall transmit signal, i.e.,

$$s(t) = \sum_{n=-\infty}^{\infty} s_n(t) = \sum_{n=-\infty}^{\infty} \sum_{k=0}^{K-1} a_k[n] g_k(t - nT_s) e^{j2\pi kFt}. \tag{2.2}$$

A block diagram of the transmitter that is based on this interpretation is shown in Figure 2.2.

In order to achieve orthogonality, OFDM uses sinusoidal pulses spectrally centered about different carrier frequencies. In the simplest case, passband pulses $g_k(t)$ are rectangular

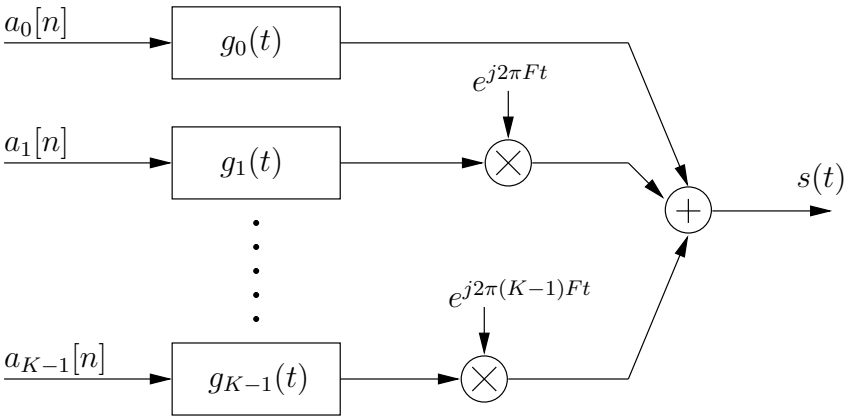

Figure 2.2: *Block diagram of the transmitter for OFDM.*

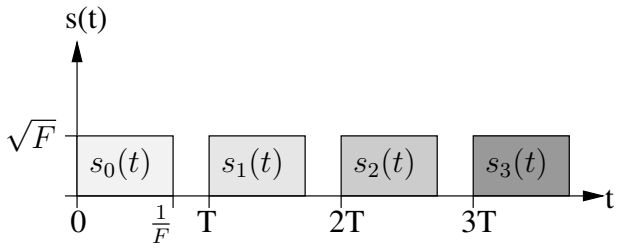

Figure 2.3: *Transmit signal with rectangular pulses.*

pulses of duration $1/F$ and amplitude $\sqrt{F}$, given by

$$g_k(t) = \begin{cases} \sqrt{F}, & 0 \leq t < \frac{1}{F} \\ 0, & \frac{1}{F} \leq t < T. \end{cases} \tag{2.3}$$

As it is shown in Figure 2.3 pulses do not overlap, as long as $T \geq 1/F$, or equivalently until $TF \geq 1$. This fundamental property has to be fulfilled in order to ensure orthogonality of pulses in time-domain. Moreover, if the above stated condition is not satisfied there does not exist any set of orthogonal pulses and therefore Inter Symbol Interference (ISI) cannot be avoided in general. Thus, in order to reduce ISI, we have to ensure that consecutive pulses are spaced as sparse as possible. On the other hand large TF reduces spectral efficiency of a system, which is inversely proportional to the effective time-bandwidth product. In practice $TF = 1.02 \ldots 1.25$ [11].

It is convenient at this point to switch signal discription from continuous to discrete-time, because most of practical implementations use discrete-time baseband processing. This transition can be seen as sampling with sampling frequency $B = KF$ and thus the sampled

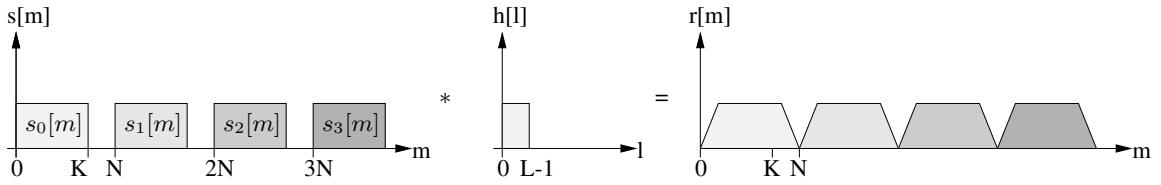

Figure 2.4: *Input-output relation for FIR channel $h[l]$. Rectangular pulses of duration K and guard interval $(N-K)$ between consecutive pulses are linearly convolved with channel impulse response $h[l]$ of duration L. As long as $(N-K) \geq (L-1)$ pulses at the output of the channel do not overlap and can be effectively demodulated by receiver, omitting ISI.*

version of the transmit signal $s[m] = s(mT_s)$ can be written as

$$s[m] = \frac{1}{\sqrt{K}} \sum_{n=-\infty}^{\infty} \sum_{k=0}^{K-1} a_k[n] e^{j2\pi \frac{km}{K}}, \tag{2.4}$$

here m is discrete time variable. The signal then passes through a multipath fading channel, modeled by a Finite-length Impulse Response (FIR) channel $h(\tau)$ of length τ_{max}. Sampling of $h(\tau)$ yields the length L discrete-time impulse response $h[l]$. Input-output relation of such FIR channel, ignoring any noise effects, is schematically depicted in Figure 2.4 and can be mathematically represented by following linear convolution

$$r[m] = (h * s)[m] = \sum_{l=0}^{L-1} h[l] s[m-l]. \tag{2.5}$$

From Figure 2.4 we conclude that ISI can be avoided if the guard interval between the consecutive samples $(N-K)$ is at least as long as the channel impulse response $(L-1)$.

At the receiver demodulation can be efficiently implemented with Fast Fourier Transformation (FFT). We recall that in discrete-time, convolution in time is equivalent to multiplication in the frequency-domain only if the signals are of infinite length or if at least one of the signals is periodic over the range of the convolution. Thus FFT of the above stated linear convolution, does not correspond to product of channel coefficients with sent samples. However, it is possible to convert linear convolution into circular, by simply prepending each OFDM symbol with replica of the last $(N-K)$ samples of the OFDM symbol, the so-called cyclic prefix. Because of the way in which the cyclic prefix is formed, the cyclically-extended OFDM symbol now appears periodic when it is convolved with the channel. Therefore, the received OFDM symbols are given by cyclic-convolution

$$\tilde{r}_n[m] = (s_n \circledast h)[m], \tag{2.6}$$

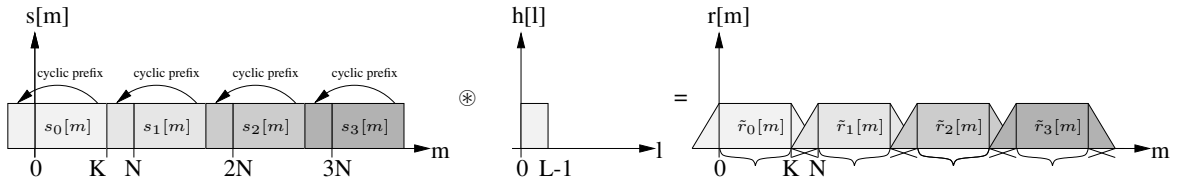

Figure 2.5: *Input-output relation for FIR channel $h[l]$. Last $(N-K)$ samples of each transmit symbol are placed in front instead of guard interval, to form cyclic prefix. Rectangular pulses with cyclic prefix are circularly convolved with $h[l]$, to form output of the channel. Received pulses $r_k[m]$ overlapp for duration of cyclic prefix $(N-K)$. But since cyclic prefix contains redundant information, it can be omitted to form not overlapping received pulses $\tilde{r}_k[m]$ of duration K.*

where

$$\tilde{r}_n[m] = \begin{cases} r[m+nN], & 0 \leq m < K \\ 0, & \text{elsewhere.} \end{cases} \tag{2.7}$$

As shown in Figure 2.6, after demodulation (FFT) cyclic convolution corresponds to multiplicative input-output relation

$$r_k[n] = H_k s_k[n] + z_k[n], \tag{2.8}$$

from which we can conclude that each subcarrier is affected by a single channel coefficient.

OFDM is attractive because of its great flexibility and ease of implementation. Specific advantages include the following:

- Due to very dense subcarrier spacing, the OFDM system has high spectral efficiency.
- Each pulse of transmit signal effectively occupies a very narrow frequency band, what makes the system suitable for dispersive channels.
- OFDM systems with cyclic prefix alters the time-dispersive (frequency-selective) channel into K parallel flat fading channels, as shown in Figure 2.6. This means that the linear distortion caused by the channel affects each pulse merely by a multiplicative factor. This fact greatly simplifies the equalization performed by receiver.
- Transmitted data, can be reobtained from received data, using simple one-tap equalizer.
- In a discrete-time setting, the transmitter (modulator) and receiver (demodulator) can be efficiently implemented by means of an IFFT and an FFT, respectively.

On the other hand, disadvantages of OFDM systems are high Peak-to-Average Power

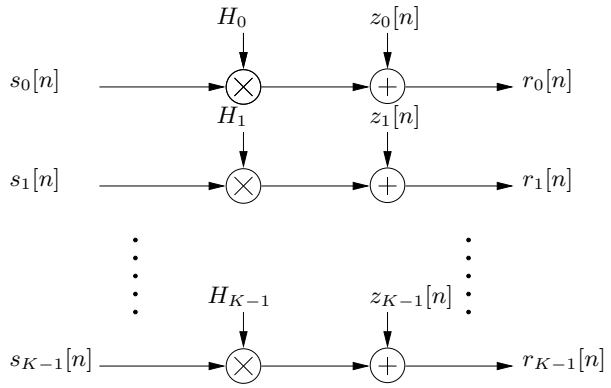

Figure 2.6: *Multiplicative input-output relation of the channel, as it is seen at the output of demodulator (FFT).*

Ratio (PARP) of the transmit signal and the need for highly accurate time-frequency synchronization (carrier recovery and symbol clock recovery) at the receiver.

2.2 Source

In contrast to real implementations, simulated transmit signals do not have to contain any specific information and thus can be represented by a random binary sequence. Random sequence is generated by the "Random Source" block that outputs a frame of M values drawn from a uniform pseudorandom distribution. Output values are selected in range between 0 and 1, and are all equally likely. Since output sequence is desired to be binary, we simply map all values that are greater than one half to "1" and to "0" otherwise.

The number of generated random bits N depends on coding rate, the utilized modulation scheme, as well as on the number of transmitted OFDM data symbols and is given as:

$$N = N_{SD} N_{sym} R N_{BPSC}, \tag{2.9}$$

where

N_{SD}	-	number of data subcarriers, which is defined to be 48 in the IEEE 802.11p,
N_{sym}	-	number of OFDM data symbols per frame,
R	-	coding rate,
N_{BPSC}	-	number of bits, corresponding to one constellation point.

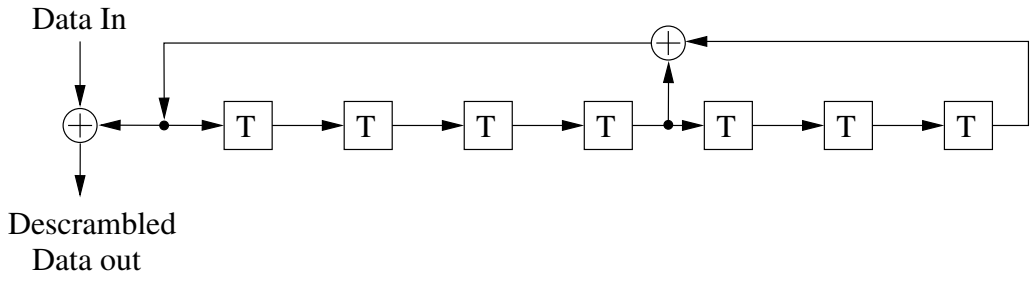

Figure 2.7: *Data scrambler.*

2.3 Encoder and Mapper

2.3.1 Scrambler

Transmitted bits are scrambled in order to randomize the data pattern, which may contain long strings of 1s or 0s. It facilitates the work of a timing recovery circuit and eliminates the dependence of a signal's power spectrum upon the actual transmitted data, making it more dispersed to meet PARP requirements. The frame synchronous scrambler uses the generator polynomial $S(x)$, as follows

$$S(x) = x^7 + x^4 + 1. \tag{2.10}$$

The scrambler is implemented with a shift register that consists of 7 delays and 2 modulo-2 adders, as shown in Figure 2.7. It repeatedly generates a 127-bit sequence for initial state 1011101. The output of the scrambler is a modulo-2 sum of the scrambling sequence and the data.

2.3.2 Encoder

The scrambled data is than passed to a convolutional encoder, which introduces, in a controlled manner, some redundancy into the bit stream. This redundancy is used for error-correcting coding which allows the receiver to combat the detrimental effects of the channel and, hence, achieve reliable communications in spite of these effects. Standard specifies rate of encoder to $1/2$, that is at each time index, the encoder takes as input one information bit u_k and produces at its output two code bits c_n.

A convolutional code introduces redundant bits into the data stream through the use of linear shift registers. Connection of the shift register taps to the modulo-2 adders is represented by generator polynomials $g_0 = 133_8 = [01011011]_2$ and $g_1 = 171_8 = [01111001]_2$. A "1" in binary vector description of generator polynomial denotes a connection to modulo-2 adder and a "0" represents no connection, as shown in Figure 2.8. Computations of convolutional encoder depend not only on the current input bit, but also on bits stored in each shift register.

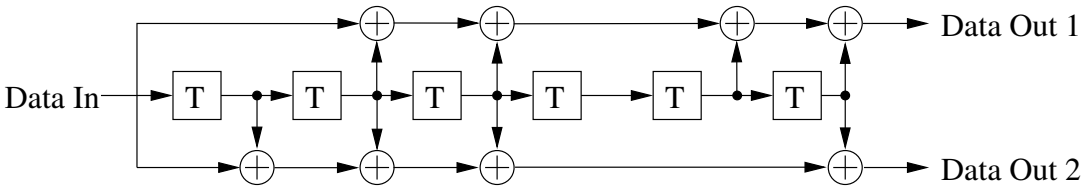

Figure 2.8: *Convolutional encoder.*

Number of information bits that potentially influence a given code bit is defined by so-called constraint length of a convolutional encoder, given as

$$K = m + 1, \tag{2.11}$$

where m is number of shift register taps. Unlike a block code that has a fixed word length, a convolutional code has no particular block size [12]. However, a convolutional code can be converted into a block code by two different standard modifications known as truncation and termination. With a terminated convolutional code the input is given by N information bits followed by m zeros bits, where m is encoder's memory order. The resulting code sequence obtained at the output of the convolutional encoder is given by first $2N$ code bits corresponding to the N data bits, followed by $2m$ further code bits that correspond to the m zero input bits but are nonzero due to the nonempty memory of encoder. Noteworthy effect of the termination procedure is to set the content of shift register in all-zero state. Other way of re-establishing the zero state that the shift register had at the beginning of the encoding is truncation. With this approach the encoder treats each frame independently, i.e., the encoder states are reset to all-zeros state at the start of each frame. The drawback of truncation method is that the last few blocks of information sequences are less protected. However, in the course of experiments it was found that the model behaves better in truncated operation mode. Also, the reason for this is still under investigation, truncation is defined as standard pattern of encoder, which can be changed manually. Note however, that changing operation mode of encoder requires changing of decoder settings as well.

Apart of so-called mother code, with coding rate $1/2$, the standard defines rates $3/4$ and $2/3$ that can be achieved by puncturing. Puncturing is procedure that derives codes of different rate from the mother code, by periodically deleting certain code bits in the code sequence of the mother code. The bits are deleted according to the given puncture vectors. Puncture vector is a pattern of 1s and 0s, with 0 indicating stolen bits, which is deleted from the mother code. The standard defines following puncture vectors $p_0 = [1110]$ and $p_1 = [110110]$, in order to achieve rates $2/3$ and $3/4$ respectively.

2.3.3 Interleaver

Interleaving is used to cope with the correlated channel noise such as burst errors or fading. The interleaver rearranges input data such that consecutive data are split among different blocks. At the receiver end, the interleaved data is arranged back into the original sequence by the de-interleaver. As a result of interleaving, correlated noise introduced in the transmission channel appears to be statistically independent at the receiver and thus allows better error correction.

One major class of interleavers are block interleavers. A block interleaver operates on one block of input bits at a time and there is no interleaving between the blocks. A block interleaver is often implemented by writing the bits into a matrix row by row and then reading them column by column. For IEEE 802.11p PHY the interleaving scheme is defined by two permutations. The first permutation ensures that adjacent bits are modulated onto non-adjacent subcarriers and the second permutation ensures that the adjacent bits are mapped alternatively onto less and more significant bits of the constellation. The block size is always equal to number of code bits in a single OFDM symbol B_{CBPS}, which depends on the signal constellation and is given in Table 2.1.

Let k denotes the index of the bit before the first permutation, i shall be the index after the first permutation and before the second permutation; and j is the index of second permutation, just prior to modulation. The first permutation is defined as:

$$i = \frac{N_{CBPS}}{16} k \bmod (16) + \text{floor}(\frac{k}{16}), \qquad k = 0, 1, \ldots, N_{CBPS} - 1. \tag{2.12}$$

Closer study reveals that the first permutation defines a matrix with 16 columns and a variable number of rows, which depends on the used modulation scheme. Input bits are written row by row and read column by column. The second permutation defines intra-column permutations, which depend on the block size and is given as

$$j = s \cdot \text{floor}(\frac{i}{s}) + (i + N_{CBPS} - \text{floor}(\frac{16 \cdot i}{N_{CBPS}})) \bmod (s), \qquad i = 0, 1, \ldots, N_{CBPS} - 1, \tag{2.13}$$

where s is a parameter dependent on the number of coded bits per subcarrier N_{BPSC}, given in Table 2.1, and is calculated according to the rule

$$s = \max(\frac{N_{BPSC}}{2}, 1). \tag{2.14}$$

Modulation	**Coding rate (R)**	**Coded bits per subcarrier (N_{BPSC})**	**Coded bits per OFDM symbol (N_{CBPS})**	**Data bits per OFDM symbol (N_{DBPS})**	**Data rate** (Mb/s)
BPSK	1/2	1	48	24	3
BPSK	3/4	1	48	36	4.5
QPSK	1/2	2	96	48	6
QPSK	3/4	2	96	72	9
16BPSK	1/2	4	192	96	12
16QAM	3/4	4	192	144	18
64QAM	2/3	6	288	192	24
64QAM	3/4	6	288	216	27

Table 2.1: *Modulation-dependent parameters*

2.3.4 Mapper

The bandwidth of the signal waveforms must be chosen in accordance with the bandwidth constraint of the channel. This means that for a simple binary modulation scheme the data rate is limited by the channel bandwidth. In order to achieve higher throughput we combine l consecutive code bits c_i into a higher-level, generally nonbinary symbol $a[k]$ that can take on $M_a = 2^l$ different values, i.e.,

$$a[k] \in \mathcal{A} = \left\{a^{(1)}, a^{(2)}, \ldots a^{(M_a)}\right\}, \qquad \text{with} M_a = 2^l. \tag{2.15}$$

Here $\mathcal{A}$ denotes the symbol-alphabet [13].

Since each symbol $a[k]$ carries l bits, for a given channel bandwidth, using M_a-ary symbols instead of the original bits we can transmit these bits $l = ld(M_a)$ times faster. Whereas the symbol rate R_s is limited by the channel bandwidth, the bit rate $R_b = lR_s$, corresponding to actual system throughput, can be arbitrarily increased by choosing l sufficiently large.

In pratice symbols $a[k]$ are mapped to a subcarrier amplitude and phase, and can be represented as a point in the complex plain. This geometrical constellation of the symbols in the complex plane is called signal constellation. The objective of the signal constellation design is to reduce the mean signal power without reducing the minimum distance between symbols and to ensure that potential symbol errors result in as few bit errors as possible. It has been shown, that for the Gaussian channel the most likely symbol errors result in symbols that are nearest neighbors of the transmitted symbol. This motivates the use of a Gray code where the binary words corresponding to neighboring symbols differ by exactly one bit and, hence, a typical symbol error results in only one bit error.

For IEEE 802.11p PHY standard defines four signal constallations: BPSK, QPSK, 16QAM and 64QAM. Conversion of code bits into complex number representing BPSK, QPSK,

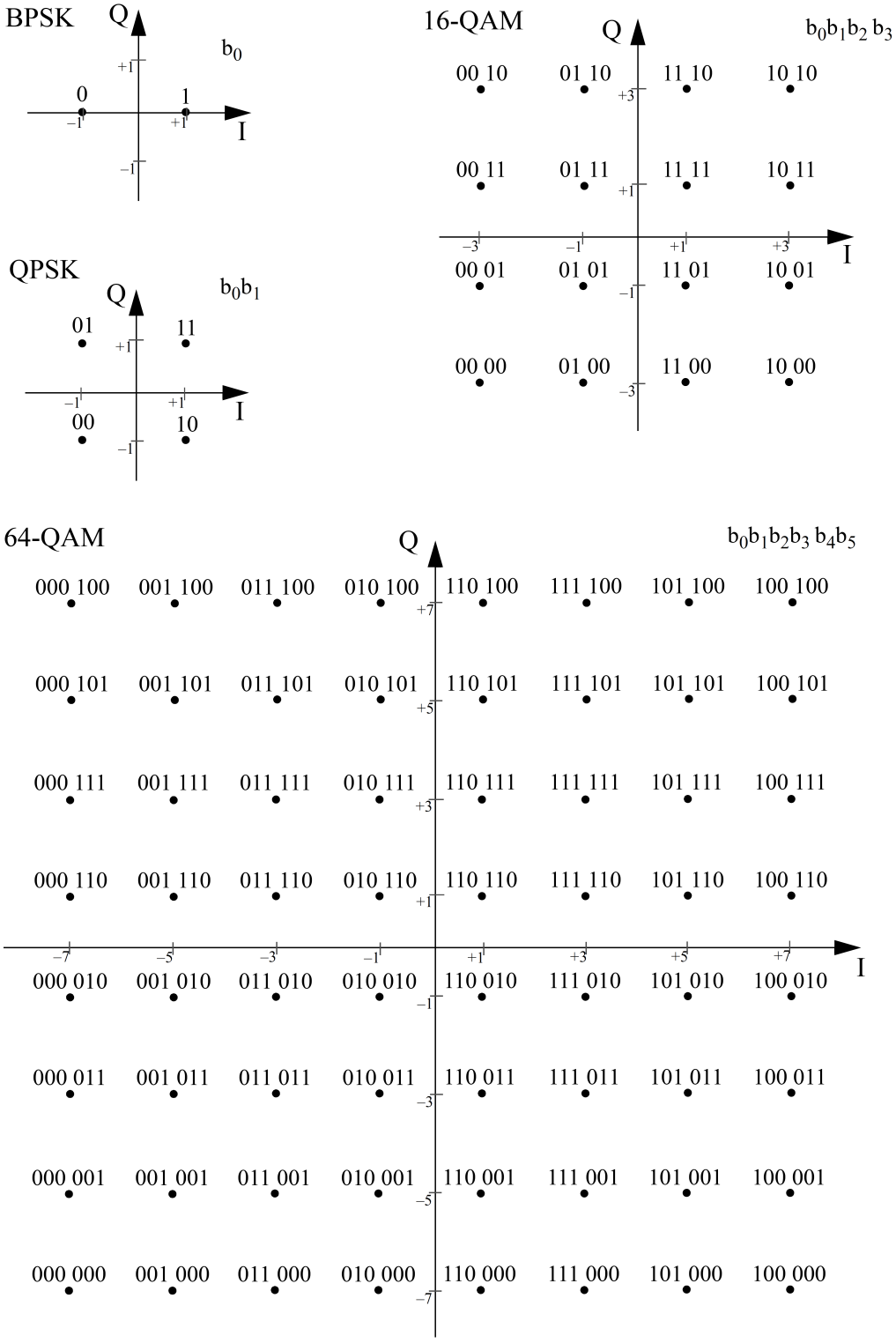

Figure 2.9: *BPSK, QPSK, 16QAM, and 64QAM constellations [10].*

Modulation	$\mathbf{K_{MOD}}$
BPSK	1
QPSK	$\frac{1}{\sqrt{2}}$
16QAM	$\frac{1}{\sqrt{10}}$
64QAM	$\frac{1}{\sqrt{42}}$

Table 2.2: *Modulation-dependent normalization factor K_{MOD}*

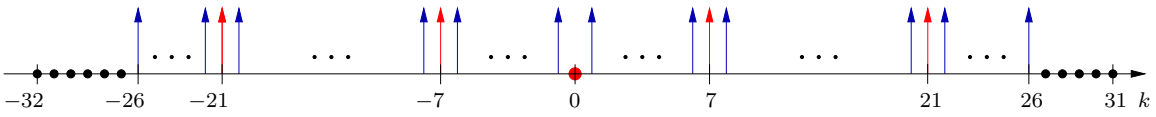

Figure 2.10: *Subcarrier allocation of the OFDM symbol.*

16QAM, or 64QAM is performed according to Gray-coded constellation mappings and is illustrated in Figure 2.9. To achieve equal average symbol power, the constellation described above are normalized by multiplying the resulting $(S_I + jS_Q)$ values by the normalization factor K_{MOD}

$$S = (S_I + jS_Q) \cdot K_{MOD}. \tag{2.16}$$

The normalization factor, depends on the modulation mode, as prescribed in Table 2.2.

2.4 OFDM Symbol Assemler

As already mentioned above, IEEE 802.11p PHY utilizes OFDM with 64 subcarriers for signal transmission. The assemble block, described in this subchapter constructs OFDM symbol by means of inserting 4 pilot- and 12 zero-subcarriers amongst the complex values d, representing BPSK, QPSK, 16QAM or 64QAM constellation points.

In order to compose the OFDM symbol complex data at the output of the modulator is first of all divided into groups of $N_{SD} = 48$ complex number, corresponding to the data subcarriers, with logical numbering 0 to 47. Logical subcarrier numbers are then mapped into frequency offset index -26 to 26, while skipping subcarriers -21, -7, 0, 7 and 21. In the next step the assembler block inserts four pilot subcarriers into positions -21, -7, 7 and 21, as well as a zero DC subcarrier between the data subcarriers by means of vertical concatenation. The DC subcarrier is not used since it can cause problems in the digital-to-analog converter. The subcarriers -32 to -27 and 28 to 32 are set to zero resulting in a guard band that considerably contributes in reducing the out of band power. Corresponding carrier allocation within the OFDM symbol is depicted in Figure 2.10.

Pilot subcarriers contain signal values that are known at the receiver. They are used by

the receiver to make coherent detection robust against magnitude and phase shift offsets, introduced by the channel, and to ensure accurate frequency and time synchronisation, which is required in order to preserve orthogonality of the subcarriers. Pilot subcarriers are constructed by taking the values $\{1, 1, 1, -1\}$ and multiplying them by the second element of sequence p_n that controlls the polarity of the pilot subcarriers.

$$\begin{aligned} p_n = \{ \quad & +1,+1,+1,+1,-1,-1,-1,+1,-1,-1,-1,-1,+1,+1,-1,+1,-1,-1,+1,+1, \\ & -1,+1,+1,-1,+1,+1,+1,+1,+1,+1,-1,+1,+1,+1,-1,+1,+1,-1,-1,+1, \\ & +1,+1,-1,+1,-1,-1,-1,+1,-1,+1,-1,-1,+1,-1,-1,+1,+1,+1,+1,+1, \\ & -1,-1,+1,+1,-1,-1,+1,-1,+1,-1,+1,+1,-1,-1,-1,+1,+1,-1,-1,-1, \\ & -1,+1,-1,-1,+1,-1,+1,+1,+1,+1,-1,+1,-1,+1,-1,+1,-1,-1,-1,-1, \\ & -1,+1,-1,+1,+1,-1,+1,-1,+1,+1,+1,-1,-1,+1,-1,-1,-1,+1,+1,+1, \\ & -1,-1,-1,-1,-1,-1,-1\} \end{aligned} \tag{2.17}$$

The sequence p_n is the cyclic extension of the 127 elements sequence and can be generated by the scrambler defined in Section 2.3.1 when the all ones initial state is used, and by replacing all 1s with -1s and all 0s with 1s. Note that the first element of the sequence p_0 is presereved and multiplies the pilot subcarriers of the OFDM symbol used in the header of the frame.

2.5 IFFT and Spectral Shaping

The data stream that consists of complex data, representing certain points of symbol constellation has to be transformed into an analog signal waveform $s(t)$ that is suited for transmission over the channel. This procedure is performed by the modulator, which in OFDM systems is implemented using a IFFT block. An OFDM system treats the symbols containing transmit data as though they are in the frequency-domain. These symbols are used as the inputs to an IFFT block that converts the signal into the time-domain. The IFFT takes in N symbols at a time, where $N = 64$ is the number of subcarriers in the system. Each of these input symbols has a symbol period of $T = 100\,\text{ns}$. Recall that the basis functions for an IFFT are N orthogonal sinusoids. These sinusoids each have a different frequency and the lowest frequency is DC. Each input symbol acts like a complex weight for the corresponding sinusoidal basis function. Since the input symbols are complex, the value of the symbol determines both the amplitude and phase of the sinusoid for that subcarrier. The IFFT output is the summation of

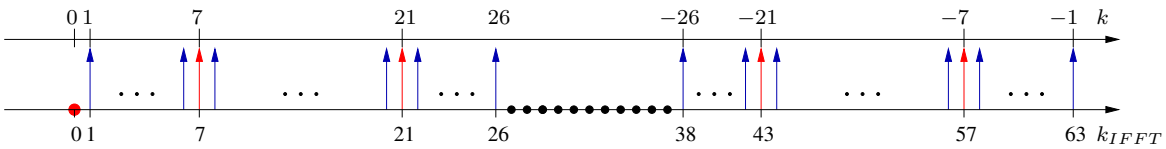

Figure 2.11: *Subcarrier rearrangement performed prior to IFFT. Axis k_{IFFT} denotes numbering of IFFT inputs, while axis k denotes initial subcarrier number as shown in Figure 2.10.*

all 64 sinusoids that makes up a single OFDM symbol [11], given as

$$s[n] = \frac{1}{\sqrt{K}} \sum_{k=0}^{K-1} S[k] e^{j2\pi \frac{kn}{K}}, \tag{2.18}$$

where $S[k]$ represents amplitude and phase of k^{th} subcarrier and is given in Equation 2.16. At the receiver, an FFT block is used to process the received signal and to convert it back into the frequency-domain as follows

$$S[k] = \frac{1}{\sqrt{K}} \sum_{n=0}^{K-1} s[n] e^{-j2\pi \frac{nk}{K}}. \tag{2.19}$$

The prefactor preceding the sums of the IFFT and FFT is merely convention and differ in some treatments. However, in order to ensure that $s[n]$ and $S[k]$ form a fourier transform pair the Parseval's theorem must hold [14], i.e.,

$$\sum_{n=0}^{K-1} |s[n]|^2 = \frac{1}{K} \sum_{k=0}^{K-1} |S[k]|^2. \tag{2.20}$$

Prior to IFFT, the subcarriers illustrated in Figure 2.10 have to be rearranged, in order to match IFFT inputs. As shown in Figure 2.11 the subcarriers 1 to 31 are mapped to IFFT inputs 1 to 31, while subcarriers -32 to -1 are copied into IFFT inputs 32 to 63 and 0 is left unchanged. Note that the normalization prefactors multiplying the sum of the IFFT and FFT in the standard SIMULINK block are given as $1/K$ and 1, respectively. Although the product of the normalization prefactors satisfies Equation 2.20, in contrast to IFFT/FFT definition stated in Equation 2.18/ 2.19 this transformation is not unitary, implying that energy contained in the modulated signal $s[n]$ is not equal to the energy of its Fourier transformation $S[k]$. For the sake of clarity in later SNR definition, implemented model specifies the unitary normalization prefactors $1/\sqrt{K}$ for both IFFT and FFT. Therefore the output of IFFT block is multiplied by the factor $\sqrt{K}$ and output of FFT by $1/\sqrt{K}$.

After the transformation in time-domain is completed each OFDM symbol is preceded by a periodic extension of itself, thus forming the cyclic prefix[1]. Duration of the cyclic prefix is given as

$$T_{CP} = \frac{T_{FFT}}{4}, \tag{2.21}$$

where $T_{FFT} = 6.4\,\mu$s is IFFT/FFT period. Hence, the cyclic prefix is just a copy of Fourier-transformed waveform corresponding to the last 16 samples of OFDM symbol.

The boundaries of each OFDM symbol are set by a multiplication by a windowing function, which is defined as a rectangular pulse of duration T_{WF}. T_{WF} may extend over the length of OFDM symbol T_{SYM}, given as $T_{SYM} = T_{FFT} + T_{CP} = 8\,\mu$s. Standard specifies $T_{WF} = 8.1\,\mu$s, in case of data OFDM symbols, that creates a small overlap between consecutive OFDM symbols, in order to smooth the transitions between them. From the implementational point of view the windowing function will be represented in discrete-time as

$$W[k] = \begin{cases} 1/2 & \text{k=1} \\ 1 & 1 \leq \text{k} \leq 80 \\ 1/2 & \text{k=81}, \end{cases} \tag{2.22}$$

with k indicating the serial number of the sample in time-domain. Thus after multiplication by the windowing function we obtain the OFDM symbol consisting of 81 samples, from which the first 17 samples represent the cyclic prefix and the rest is a time-domain version of 64 subcarriers shown in Figure 2.10. The first and the last sample of each OFDM symbol are then halved and summed up with the last sample of the preciding and first sample of the succeeding OFDM symbols respectively, thus creating an overlap of duration $0.1\,\mu$s between consecutive symbols.

2.6 Constructing PPDU Frame

During transmission, the PSDU shall be provided with a PLCP preamble and header to create the PPDU frame. As shown in Figure 2.12 the format for the PPDU includes the OFDM PLCP preamble, OFDM PLCP header, PSDU, tail and pad bits. The PLCP preamble field consists of ten short symbols and two long symbols and is used for synchronization and

[1]For more detailed information about use of cyclic prefix in OFDM systems see Subchaper 2.1

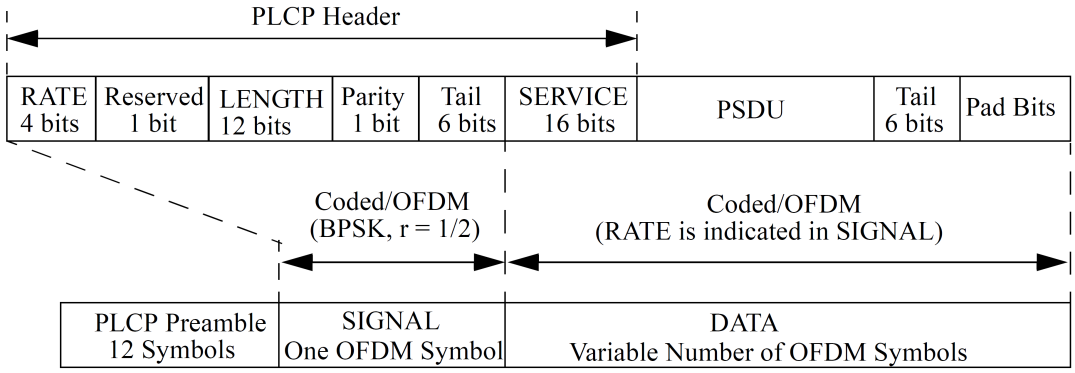

Figure 2.12: *PPDU frame format [10].*

channel estimation. A short OFDM training symbol is given by sequence:

$$\begin{aligned} S \;= \sqrt{\tfrac{13}{6}}\; \{\, & 0,0,0,0,0,0,0,0,+1+j,0,0,0,-1-j,0,0,0,+1+j,0,0,0,-1-j, \\ & 0,0,0,-1-j,0,0,0,+1+j,0,0,0,0,0,0,0,-1-j,0,0,0,-1-j,0,0, \\ & 0,+1+j,0,0,0,+1+j,0,0,0,1+j,0,0,0,1+j,0,0,0,0,0,0,0\,\} \end{aligned} \tag{2.23}$$

The multiplication factor $\sqrt{(13/6)}$ is in order to normalize the average power of the resulting OFDM symbol, which utilizes 12 out of 64 subcarriers, as shown in Figure 2.13 (a). Hereafter subcarriers are modulated as described in Subchapter 2.5 and the single period of the short training sequence is extended periodically for 161 samples and then multiplied by the window function

$$W[k] = \begin{cases} 1/2 & \text{k=1} \\ 1 & 1 \leq \text{k} \leq 160 \\ 1/2 & \text{k=161}, \end{cases} \tag{2.24}$$

Finally, we can conclude from Figure 2.13 (b) that the training sequence S, given in Equation 2.23 yields ten short training symbols t_1 to t_{10}, each of duration $1.6\,\mu$s, which can be used by receiver for signal detection, diversity selection, coarse frequency offset estimation and timing synchronization. Note that short training symbols are not prepended with cyclic prefix.

Two long training symbols can be used for channel and fine frequency offset estimation

R1-R4	Rate Mb/s
1101	3
1111	4.5
0101	6
0111	9
1001	12
1011	18
0001	24
0011	27

Table 2.3: *Content of the rate field, with R1-R4 corresponding to the first four bits of signal field.*

and are given by sequence:

$$\begin{aligned} L \;=\; \{\, & 0,0,0,0,0,0,+1,+1,-1,-1,+1,+1,-1,+1,-1,+1,+1,+1,+1,+1,+1, \\ & -1,-1,+1,+1,-1,+1,-1,+1,+1,+1,+1,0,+1,-1,-1,+1,+1,-1,+1, \\ & -1,+1,-1,-1,-1,-1,-1,+1,+1,-1,-1,+1,-1,+1,-1,+1,+1,+1,+1, \\ & 0,0,0,0,0\,\} \end{aligned} \tag{2.25}$$

The subcarriers plotted by sequence L are modulated, periodically extended and multiplied by the window function $W[k]$ previously defined for short training symbols (see Equation 2.24). In this manner the implemented model constructs two long training OFDM symbols, each of duration $6.4\,\mu$s, prepended with a cyclic prefix of duration $3.2\,\mu$s, which is doubled as compared with duration of cyclic prefix of data OFDM symbol. The reason for this is that the cyclic prefix contributes to both long training symbols and instead of prepending each symbol with cyclic prefix of duration $1.6\,\mu$s, as it is done for data symbols, it is appended just once infront of the first symbol.

The PLCP preamble field is followed by the signal field, which contains the rate and the length fields that are required for decoding the data part of frame. The first 4 bits constitutes the rate field that conveys information about type of modulation and the coding rate, according to the values in Table 2.3. Bits 6 to 17 are assigned for the length field, given by a 12-bit integer that indicates the number of octets in the PSDU that the MAC layer is currently requesting the PHY to transmit. This value is used by PHY to determine the number of octet transfers that will occur between the MAC and the PHY after receiving a request to start transmission. Bits 5 and 18 are are reserved for future use, while the bits $19 - 24$ constitute the signal tail and shall be set to zero.

The encoding of signal OFDM symbol is performed using a convolutional encoder and interleaver defined in Sections 2.3.2 and 2.3.3. For transmission it is mapped to the most

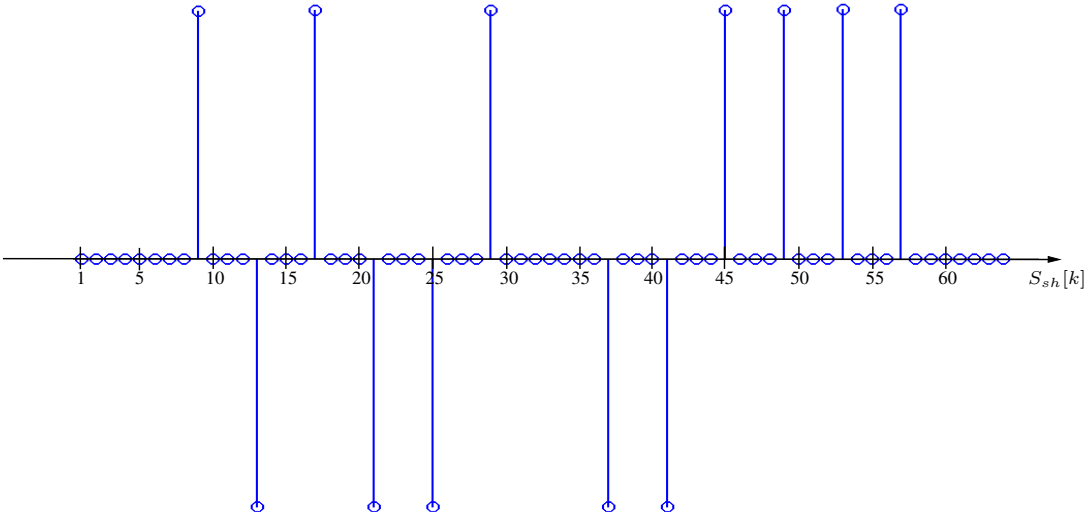

(a) *Short training sequence in frequency-domian*

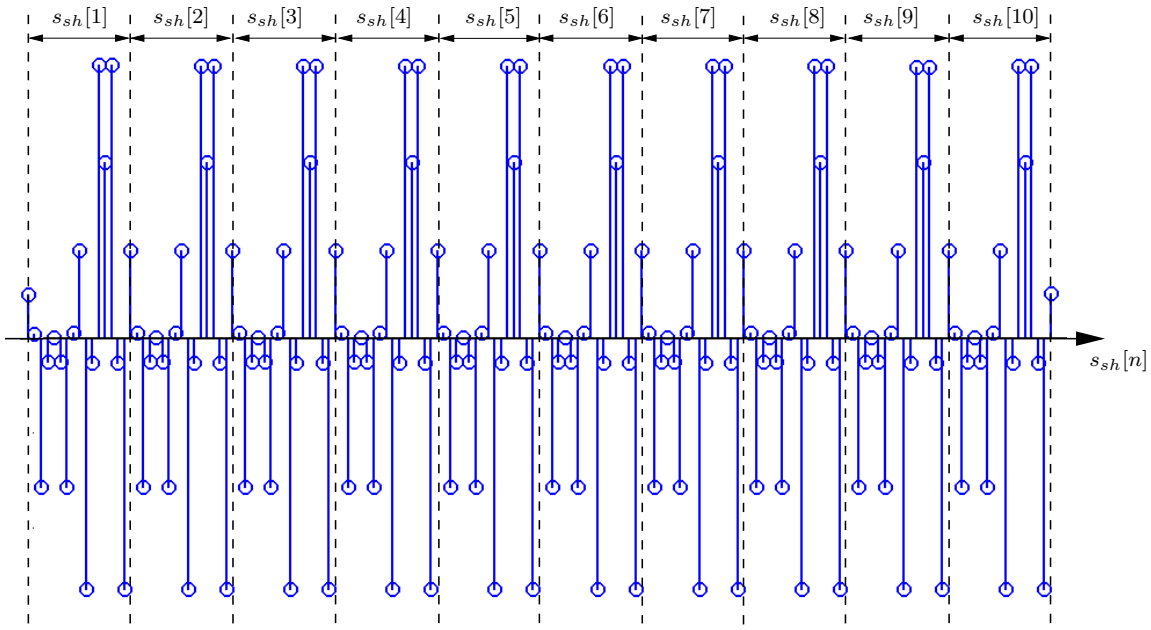

(b) *Short training sequence in time-domain, multipliyed by window function*

Figure 2.13: *Generation of short training sequence.*

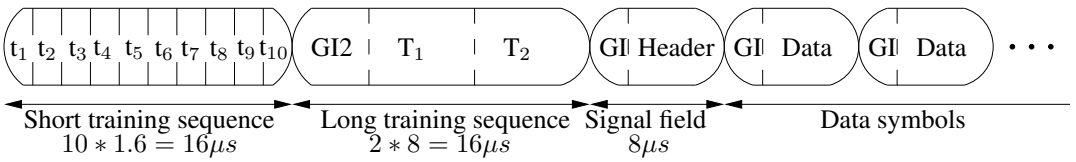

Figure 2.14: *Frame structure.*

robust symbol constellation, BPSK with coding rate $R = 1/2$, modulated with IFFT, cyclically extended and multiplied by the window function, as described in Subsection 2.5 for data OFDM symbols. Finally PPDU frame can be assembled by simply appending train of training, signal field and data symbols one after another, as shown in Figure 2.14.

3

Channel

In all types of wireless communications, the transmission medium is the radio channel between transmitter and receiver. The signal propagates via a number of different paths, that either have a Line-of-Sight (LOS) or Non-Line-of-Sight (NLOS) connection between transmitter and receiver. Furthermore the signal can be reflected, scattered, and diffracted by different objects in the environment. All this and many other conditions that determine the different multipath components have a great impact on the performance (e.g., capacity and reliability) of vehicular communication networks and thus have to be investigated. In many circumstances it is too complicated to consider all slight effects introduced by the propagation channel and therefore simplified channel models that reflect merely the most important properties of channels in parametric form are developed.

Since accurate and realistic models of the propagation channel are crucial for testing and performance optimization of developed models, in this chapter we describe the basic mechanisms that govern signal propagation in wireless environments and outline various modeling parameters. First and foremost the Additive White Gaussian Noise (AWGN) channel has been implemented in order to validate the model performance by means of precalculated numerical BER vs. SNR relations. However, due to existence of a multitude of propagation paths, where the signal can be reflected or scattered along its way we can not consider the AWGN channel as realistic scenario in wireless environments. In order to investigate the model dependence on the number of propagation paths from the transmitter to the receiver, Section 3.2 introduces the so-called block-fading channel, that can be viewed as a

frequency-selective channel model. In addition to multipath issue, signal propagating in vehicular networks suffers dramatically from Doppler shift, introduced by high relative velocities. The time-variant channel model presented in Section 3.3 addresses this issues and facilitates deeper understanding of the model behavior in propagation environments with strong multipath components and fast motions.

Prior to the discussion of the above mentioned channel models it is important to underline the Signal-to-Noise-Ratio (SNR) definition, assumed in the current implementation. For the bandlimited, power-constrained AWGN channel with bandwidth B_T, mean signal power P_s, and noise power spectral density $N_0/2$, the channel SNR can be interpreted as:

$$SNR_{ch} = \frac{P}{N_0 B_T}, \tag{3.1}$$

where the quantity $N_0 B_T$ is the mean noise power within the signal band: $\frac{1}{2\pi}\int_{-\Omega_T}^{\Omega_T} S_N(j\omega)d\omega$ [12]. In contrast to single-carrier systems, the total channel bandwidth of multi-carrier systems is given by a product of utilized subcarriers K and frequency separation between subcarriers F. Therefore, the channel SNR is defined as follows

$$SNR_{ch} = \frac{P}{N_0 K F}. \tag{3.2}$$

Recall that each OFDM symbol consists of $K = 64$ subcarriers[1], out of which 12 subcarriers are zeros, corresponding to frequency guard band and DC (see Figure 2.10). Nulling of the high frequency subcarriers introduces oversampling and therefore the channel bandwidth KF is larger than the bandwidth actually occupied by data and pilot subcarriers $\tilde{K}F$. Hence, the channel SNR, and the SNR obtained after downsampling in frequency-domain are not equal are related as follows

$$\frac{SNR_{ch}}{SNR} = \frac{\frac{P}{N_0 K F}}{\frac{P}{N_0 \tilde{K} F}} = \frac{\tilde{K}}{K}, \tag{3.3}$$

or expressed logarithmically

$$10\log_{10}\frac{SNR_{ch}}{SNR} = SNR_{ch,dB} - SNR_{dB} = 10\log_{10}\frac{\tilde{K}}{K}. \tag{3.4}$$

Substituting the total number of subcarriers $K = 64$ and the number of non-zero subcarriers $\tilde{K} = 52$, we obtain the correction term, introduced in all channel models in order to address

[1]Here we do not consider cyclic prefix, since redundant information carried on this 16 non-zero subcarriers will be omitted by receiver immediately after demodulation

oversampling issues

$$SNR_{ch,dB} = SNR_{dB} + 10\log_{10}\frac{\tilde{K}}{K} = SNR_{dB} + 10\log_{10}\frac{52}{64} = SNR_{dB} - 0.9018. \quad (3.5)$$

3.1 AWGN Channel

The AWGN channel is a reasonably accurate model for many practical channels, what can be explained by the central limit theorem [13], which states that under certain conditions the superposition of n independent random variables yields a Gaussian random variable as $n \to \infty$. The AWGN channel attenuates the transmit signal, causes phase rotation, and adds Gaussian distributed noise. Attenuation and phase rotation are temporally constant, and are thus easy taken in account [15]. The receive signal can be modeled as:

$$r[n] = \alpha s[n] + z[n], \quad (3.6)$$

where α is a complex attenuation $|\alpha|e^{j\phi}$, $r[n],\ s[n]$ and $z[n]$, are the received signal, the transmitted signal and the noise components corresponding to k^{th} subcarrier at the time instance n, respectively. It can be shown (see [13]), that $z[n]$ is a stationary, zero-mean, circularly symmetric random process, with the real part $z_R[n]$ and the imaginary part $z_I[n]$ statistically independent and Gaussian distributed with identical variances equal to $\sigma_z^2/2$. Hence, the Probability Density Function (PDF) of $z[k]$ is

$$\begin{aligned} f_z(z) &= f_{z_R}(z_R) f_{z_I}(z_I) \\ &= \frac{1}{\sqrt{2\pi\sigma_z^2/2}}\exp(-\frac{1}{2}(\frac{z_R}{\sigma_z/\sqrt{(2)}})^2)\frac{1}{\sqrt{2\pi\sigma_z^2/2}}\exp(-\frac{1}{2}(\frac{z_I}{\sigma_z/\sqrt{(2)}})^2) \\ &= \frac{1}{\pi\sigma_z^2}\exp(-\frac{z_R^2 + z_I^2}{\sigma_z^2}) \\ &= \frac{1}{\pi\sigma_z^2}\exp(-\frac{|z|^2}{\sigma_z^2}), \end{aligned} \quad (3.7)$$

where σ_z^2 is the noise variance, which equals the noise mean power, since $z[k]$ is zero-mean. [2]

In the developed model white Gaussian noise is added by means of the standard AWGN channel block, which adds complex Gaussian noise and produces a complex output signal, if the input to the block is complex. This is always the case, since time-domain signal at the output of the modulator (IFFT) is given by a sequence of complex numbers, although symbols itself might be real. As e.g., in case of BPSK signal constellation.

[2] Note, that $f_z(z)$ is a function of $|z|$ and thus circularly symmetric about the origin of the complex plain.

3.2 Block-Fading Channel

The presence of multiple random reflectors and scatterers along the signal propagation path induce multiple copies of the transmitted signal, each having a different amplitude, phase and delay, this copies are then added at the receiver creating either constructive or destructive interference. Since the received signal, represented by multitude of its copies, is spread in time the channel is said to be time-dispersive or also called frequency-selective. A frequency-selective fading channel cannot be described by a simple attenuation coefficient, as in the case of an AWGN channel (see Equation 3.6), but rather the details of the channel transfer function must be modeled. Assume all components of the wireless propagation system (transmitter, receiver and interacting objects) are static, then the channel is time-invariant and can be described by its impulse response $h(\tau)$. In this case the theory of Linear Time Invariant (LTI) systems is applicable [15] and thus the physical channel can be interpreted as a linear filter with input-output relation

$$r(t) = \sum_{i=0}^{L-1} h_i s(t - \tau_i), \tag{3.8}$$

where L is the number of resolvable paths, τ_i is path delay and h_i is time-invariant channel impulse response. However, due to the presence of motion at the transmitter, the receiver or the surrounding objects, the multipath channel changes over time and thus the channel impulse response $h(t, \tau)$ is time-varying as well. For this reason the theory of Linear Time Variant (LTV) system must be used [15], which imposes following input-output relation

$$r(t) = \sum_{i=0}^{L-1} h_i(t) r(t - \tau_i(t)). \tag{3.9}$$

Since any wireless system, and thus the channel we are interested in, is band-limited the impulse-response can be represented by a sampled version of continuous impulse response $h(t, \tau_i)$, called tapped delay line. The impulse response is then written as:

$$h(t, \tau) = \sum_{i=0}^{L-1} c_i(t) \delta(\tau - \tau_i), \tag{3.10}$$

here L is number of taps, corresponding to the number of multipath components, $c_i(t)$ are the time-dependent complex amplitude coefficients for the taps, and τ_i is the delay of i^{th} path. Commonly taps of tapped delay line are uniformly spaced, i.e., $\tau_i = i \cdot \Delta\tau$, where the distance between the taps $\Delta\tau$ is determined by the Nyquist theorem [13].

The tapped delay line can be seen as a discrete-time representation of the Power-Delay Profile (PDP) that is a function determined by the average power associated with each path.

The most important parameter derived from the PDP is channel the Delay Spread (DS) that is given as a function of the time differences between the arrival of the significant paths. The DS can be characterized through different metrics, although the most common one is the Root Mean Square Delay Spread (RMSDS), that is given as the second centered moment of DS spectrum [15]. A larger DS implies increased frequency selectivity and a smaller coherence bandwidth. To put it in another way, if DS of the channel is longer than the length of the cyclic prefix, simple multiplicative input-output relation for the channel in frequency-domain (see Equation 2.8) does not hold any more, therefore, consecutive OFDM symbols overlap resulting in ISI.

Propagation in a scattering environment is often characterized by an impulse response with exponentially-decaying PDP, given as [16]

$$P_h(t) = \begin{cases} \exp(-\frac{t}{\sigma_t}) & t \geq 0 \\ 0 & \text{otherwise} \end{cases}, \tag{3.11}$$

where $P_h(t)$ is the PDP of the channel, σ_t is the RMSDS of the exponential-shaped PDP. The implemented channel model described in this subchapter is as well approximated by a one-sided exponential function, given in form of tapped delay line. In practice, this can be achieved by sampling of PDP function with sampling time mT_s. This results in discrete propagation delays T_s, corresponding to equidistantly spaced taps of a tapped delay line. Each tap is characterized by the path gain of the m^{th} discrete propagation path, or equivalently weight of m^{th} delay tap and is given as [17]

$$p_h[m] = \gamma \sqrt{\exp(-\frac{mT_s}{\sigma})}. \tag{3.12}$$

The multiplicative factor $\gamma = 1/\sqrt{\sum_{m=0}^{L-1} |p_h[m]|^2}$ in Equation 3.12 has been introduced in order to normalize the sum of squares of all gain coefficient, corresponding to power of multipath components, to unity, i.e., $\sum_{m=0}^{L-1} |p_h[m]|^2 = 1$. The channel length $(L-1)$, or equivalently the maximum value of tap delay given by the DS length and RMSDS (σ) are both user defined parameters and can vary arbitrary.

Further restriction imposed on tapped delay line structure of the implemented channel model is that the amplitudes of all taps are Rayleigh distributed. This is a commonly used fading model for wireless NLOS systems, since in-phase and quadrature components of the received signal are the sums of many random variables, describing all reflection, diffraction, scattering process that determine the different multipath components. As already mentioned in Section 3.1, the PDF of such a sum is Gaussian distributed (see Equation 3.7). For this reason the weights $p_h[m]$ of the individual components (taps) of each instantiation are mul-

tiplied with independent complex Gaussian variables, representing in-phase and quadrature components of the received signal. Starting with statistics of real and imaginary parts, [15] derives statistics of amplitude and phase of received signal. The joint PDF of each component is a product of uniformly distributed phase $\psi \in (-\pi, \pi]$, with PDF $f_\psi(\psi) = 1/2\pi$ and Rayleigh distributed amplitude $r \in [0, \infty)$, with PDF $f_r(r) = r/\sigma^2 \cdot \exp[-r^2/2\sigma^2]$ and is given as:

$$f_{r,\psi}(r,\psi) = \begin{cases} \frac{r}{2\pi\sigma^2}\exp(-\frac{r^2}{2\sigma^2}) & 0 \leq r < \infty, -\pi \leq \psi \leq \pi \\ 0 & \text{otherwise} \end{cases}. \tag{3.13}$$

In the very last step of the frequency-selective fading simulation model we form a received sequence $r[n]$ by convolving the transmitted sequence $s[n]$ with Rayleigh distributed channel coefficients $h[m]$, given by taps of exponential PDP defined in Equation 3.12 and adding circular symmetric complex white Gaussian noise $z[n]$ with zero-mean and variance σ_z^2

$$r[n] = (h[m] * s[n]) + z[n], \tag{3.14}$$

here $[n]$ is the discrete-time index and $[m]$ is the number of certain tap of the exponential PDP, as defined in Equation 3.12. Note, that the channel coefficients $h[m]$ are not time-dependent, thus the channel is represented by a simple LTI filter.

To complete the discussion of the implemented block-fading channel model, we have to define periodicity of channel variations, or in other words time period over which channel coefficients are constant. As already mentioned above, due to presence of motion, the multipath channel changes over time and thus the channel impulse response cannot be always interpreted as a LTI filter. However, for block fading channel model, introduced in [18], the noise severity remains constant in blocks of M consecutive transmitted symbols, but is independent from block to block. Meaning for implemented model, that the fading varies slowly in time and the channel coefficients remains constant over one OFDM frame. However, channel realizations for consecutive frames are independent, as shown in Figure 3.1. This assumption is very restrictive, but still, the block-fading channel model matches certain real channels very well.

3.3 Time-Variant Channel

The assumption, that the channel coefficients remain constant within one OFDM frame is rarely fulfilled in practice. Commonly we have to deal with time-variant channels that vary significant over the duration of each OFDM frame. For this reason the developed physical

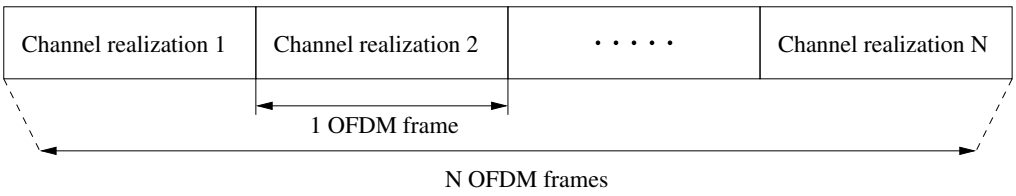

Figure 3.1: *Block-fading channel model.*

layer model includes time-variant channels that introduce time selectivity of channel coefficients in addition to frequency selectivity described in Section 3.2.

The variation of a wireless channel over the duration of a data block is caused by several impinging wavefronts, each with potentially different frequency shift. The shift of the received frequency, called the Doppler shift occurs when the receiver, the transmitter or the interacting objects are in relative motion. Hence, if the receiver moves away from the transmitter with speed v the distance d between transmitter and receiver increases with that speed and the received signal can be described as

$$\begin{aligned} E(t) &= E_0 \cdot \cos(2\pi f_c t - k_0[d_0 + vt]) \\ &= E_0 \cdot \cos(2\pi t[f_c - \frac{v}{\lambda}] - k_0 d_0), \end{aligned} \tag{3.15}$$

where k_0 is a wavenumber $2\pi/\lambda$ and d_0 is the distance at time $t = 0$ [15]. The frequency of the received oscillation f_c is thus decreased by Doppler shift v/λ. Hence Doppler shift is defined as:

$$\nu = -\frac{v}{\lambda} = -f_c \cdot \frac{v}{c_0}, \tag{3.16}$$

here f_c is the carrier frequency and c_0 is the speed of light. In Equation 3.16 we have assumed that the direction of receiver movement is aligned with the direction of wave propagation. If that is not the case, the Doppler shift is determined by the speed of movement in the direction of wave propagation, $v \cdot \cos(\phi)$. The Doppler shift is then:

$$\nu = -\frac{v}{\lambda}\cos(\phi) = -f_c \cdot \frac{v}{c_0}\cos(\phi) = -\nu_{max}\cos(\phi), \tag{3.17}$$

with ϕ the arrival angle of the received signal component and $\nu_{max} = f_c \cdot v/c_0$ the maximum Doppler shift. Since the relative motion v is fairly small compared to the speed of light c_0, one can conclude that the Doppler shifts are small (typically 1 Hz-1 kHz) as well and could be easily eliminated by the local oscillator at the receiver. The important point however, is that the different multipath components have different Doppler shifts, that introduce frequency dispersion (time selectivity) in addition to frequency selectivity.

For the sake of clearness, let us first assume that the channel is frequency-flat, meaning that there exist only one path between transmitter and receiver. Then the time-variant flat-fading channel $h[n]$[3] can be approximated by e.g., the classical or Jakes spectrum, statistical simulation model of which is introduced in [19], as follows

$$h[n] = \frac{1}{\sqrt{2}}(h_c[n] + jh_s[n]) \tag{3.18}$$

with:

$$h_c[n] = \frac{2}{\sqrt{A}} \sum_{i=1}^{A} cos(\psi_i) \cdot \cos(2\pi\nu n \cos\alpha_i + \phi) \tag{3.19}$$

and:

$$h_s[n] = \frac{2}{\sqrt{A}} \sum_{i=1}^{A} sin(\psi_i) \cdot \cos(2\pi\nu n \cos\alpha_i + \phi), \tag{3.20}$$

where A is the number of propagation paths, ψ_i is the random variable introduced to ensure that the in-phase and quadrature components of $h[n]$ are statistically uncorrelated and have equal power, ϕ_i is the initial phase associated with i^{th} propagation path, ν is the Doppler shift and α_i is the angle of the incoming wave and is given as:

$$\alpha_i = \frac{2\pi i - \pi + \theta}{4A} \qquad \text{for } i \in 1, \ldots, A, \tag{3.21}$$

with the random variable θ is introduced in order to normalize the radian Doppler frequencies. Note, that ψ_i, ϕ, and θ are independent and uniformly distributed on $[\pi, \pi)$ for all i.

In the next step we introduce frequency-selectivity, resulting from multipath propagation in addition to time-variations of the channel described by the Jakes spectrum. Channel coefficients $h[m, n]$ are then formed by simple multiplication

$$h[m, n] = h[m] \cdot h[n]. \tag{3.22}$$

Here the influence of multipath propagation is introduced by Rayleigh distributed channel coefficients $h[m]$, given by taps of exponential PDP defined in Equation 3.12. Furthermore, Doppler shift introduced by relative motion in the channel forces each multipath component to vary over the time. This effect is achieved by multiplying each tap of PDP by independent Jakes spectrum $h[n]$. The resulting received signal $r[n]$ at the output of time-variant channel $h[m, n]$ is then given as:

$$r[n] = h[m, n] * s[n] + z[n], \tag{3.23}$$

with $z[n]$ being circular symmetric complex white Gaussian noise with zero-mean and vari-

[3]Note, that n represents discrete-time index in this notation.

Tap	Channel A		Channel B	
	Relative delay (ns)	**Average power (dB)**	**Relative delay (ns)**	**Average power (dB)**
1	0	0.0	0	−2.5
2	310	−1.0	300	0.0
3	710	−9.0	8900	−12.8
4	1090	−10.0	12900	−10.0
5	1730	−15.0	17100	−25.2
6	2510	−20.0	20000	−16.0

Table 3.1: *ITU channel model for vehicular test environments.*

ance σ_z^2. It is necessary to underline two important differences between input-output relation of the time-invariant channel given in Equation 3.14 and the time-variant channel in Equation 3.23. First and foremost the channel coefficients in Equation 3.23 change over time that involves time-varying convolution of transmitted signal $s[n]$ and channel coefficients $h[m, n]$.

As already mentioned above realistic environments are too complex to model accurately. Most simulation studies use empirical models that have been developed based on measurements taken in various real environments. Up to now multipath fading was modeled as a tapped-delay line with uniform delays and exponentially-decaying PDP, moreover channel length $L - 1$ is restricted to be not longer than length of cyclic prefix $N - K$. However in real channels these assumptions do not necessarily hold. The commonly used set of empirical channel models is that specified in [20]. The recommendation specifies three different test environments: Indoor office, outdoor-to-indoor pedestrian, and vehicular - that we are actually interested in. Since the DS can vary significantly, the recommendation specifies two different DSs: low DS(A), and medium DS (B). Table 3.1 lists the relative delay and average power of each tap of ITU channel model for vehicular test environment, which are in addition grafically represented in Figure 3.2.

We should carefully note, that the tap locations for channel A don't match sampling grid of our discrete-time simulation, which is given by the sampling period $T_s = 100\,\text{ns}$. The tap locations can be adjusted using one of the following methods:

- *Rounding to the nearest neighbor* algorithm simply selects the value of the nearest point on the sampling grid of discrete simulation, and does not consider the values of other neighboring points at all, yielding a piecewise-constant interpolation. This method leads to error that are smaller the higher the new sampling rate is.

- *Sinc interpolation* method spreads energy of each unadjusted tap between taps adjusted to the sampling rate of the physical layer model using the sinc function. The sinc function is defined as $\text{sinc}(x) = \sin(\pi x)/(\pi x)$. Energy of each unadjusted tap contributes

to the overall energy as sinc function centered on that tap. The sinc function is scaled to match the average power of the tap. The frequency of the sinc function is set to match the sample rate $T_s = 100\,\text{ns}$. The overall signal is the sum of all of the sinc functions of all of the samples.

Sinc interpolator yields more precise results, compared to the nearest neighbor method and for this reason is exerted to adjust taps of channel A to the sampling rate of the implemented physical layer model. Due to smoothing effect of sinc-interpolation, tapped delay line representing channel A is not longer given by just 6 taps, as defined in Table 3.1 but rather is smoothed over infinitely many taps. However, only the first 30 taps of interpolated tapped delay line are used to form new representation of channel A model, since weight of residual taps is neglectably small.

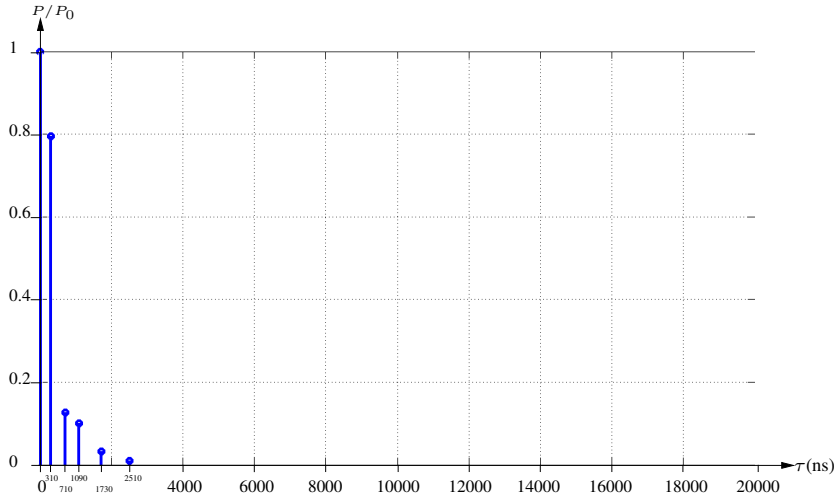

(a) *Channel A*

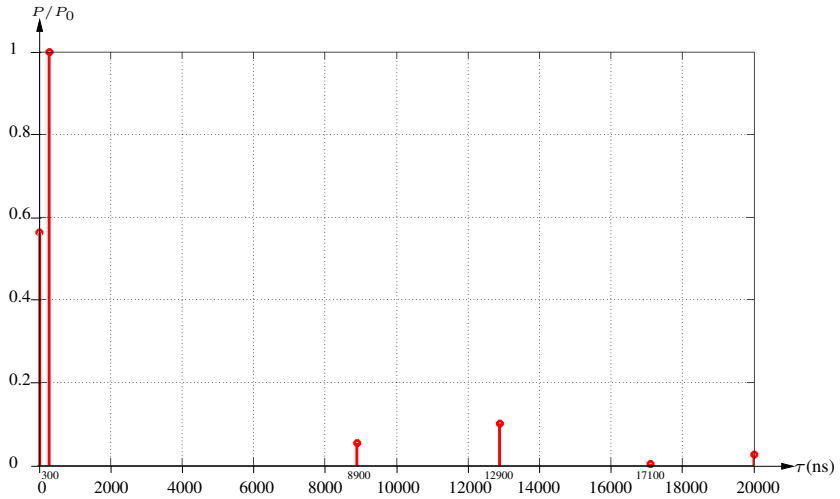

(b) *Channel B*

Figure 3.2: *ITU channel models for vehicular test environments. Note, that here we show relative power of each tap, rather than value in dB, as defined in Table 3.1*

.

4

Receiver

In Chapter 2 we have described all essential steps that are performed at the transmitter side in order to protect signal against corruptive effects introduced by a wireless communication channel. As result of this transformation the binary data sequence was mapped onto signal waveform that has specific structure, previously referred as frame. Apart of payload each frame conveys a preamble, based on which the receiver first estimates the channel coefficients and thereafter reverses the processing performed at the transmitter in a block-wise manner, as shown in Figure 4.1.

This chapter takes a closer look at the main receiver blocks and describes how they are implemented in the model. Thus, we start with the Serial-to-Parallel (S/P) block that divides received signal into blocks of 80 samples and separates the preamble and the signal field from payload. After demodulation with the FFT algorithm, cyclic prefix, pilots and frequency guard band are removed from each OFDM symbol and two long training symbols are used to estimate the channel coefficients. Based on the estimated channel coefficients the equalizer compensates the fading effects introduced by the channel and relays the samples to the decoder. Finally the received and decoded binary data stream is compared to the transmitted one, in order to derive overall error ratio statistics.

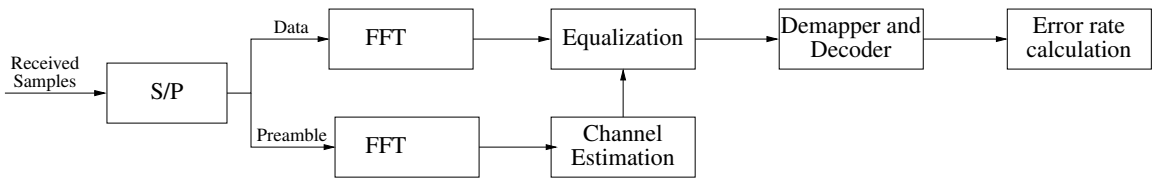

Figure 4.1: *Block diagram of receiver.*

4.1 Demodulator

The received signal is formed out of successive PPDU frames, each of which has specific structure shown in Figure 2.14. Each frame is processed by the S/P block, that divides signal into blocks of 80 samples, out of which the first two blocks correspond to the ten short train symbols, the third and the forth blocks are long train symbols, fifth block conveys signal field and the rest are data symbols. Thereafter time-domain symbols have to be demodulated to yield 64 parallel subcarriers. Prior to demodulation, we have to remove the cyclic prefix by merely ignoring first 16 samples of each symbol. As it was already shown in Section 2.5 modulation and demodulation in OFDM systems can be efficiently implemented by means of IFFT and its counterpart FFT. At the transmitter frequency-domain data was converted to time-domain data, by simple correlation of the frequency-domain input data with orthogonal basis functions of IFFT, which are sinusoids at certain frequencies. FFT at the receiver perform the inverse operation, given in standard SIMULINK block as

$$S[k] = \sum_{n=0}^{K-1} s[n] e^{-j2\pi \frac{nk}{K}}. \tag{4.1}$$

Recall that in Section 2.5 we have multiplied the output of the IFFT block by the factor $\sqrt{K}$ in order to ensure that the IFFT/FFT transformation is unitary and thus the energy contained in the modulated signal $s[n]$ is equal to the energy of its Fourier transformation $S[k]$. To ensure that the Parseval's theorem holds, implying that $s[n]$ and $S[k]$ form a valid Fourier transform pair, the output of FFT block is multiplied by $1/\sqrt{K}$.

At the output of the FFT block the zero-frequency component is in the upper-left corner of the spectrum and the guard band is in the middle as shown in Figure 2.11. We rearrange subcarriers by swapping the left and right halves of the spectrum and moving the zero-frequency component to the middle. Ideally, the FFT output will be the original samples that were sent to the IFFT at the transmitter. When plotted in the complex plane, the FFT output samples will form a constellation, which might significantly differ from the regular shape of constellation introduced in Section 2.3.4, due to corruptive effects of the channel. Thus, prior to any receiver processing that uses the concept of a constellation, such as symbol slicing and demapping, signal equalization shell be performed.

4.2 Channel estimator

As for any other coherent wireless system, the operation of developed physical layer model requires an estimate of the channel transfer function. As already mentioned in Section 2.1

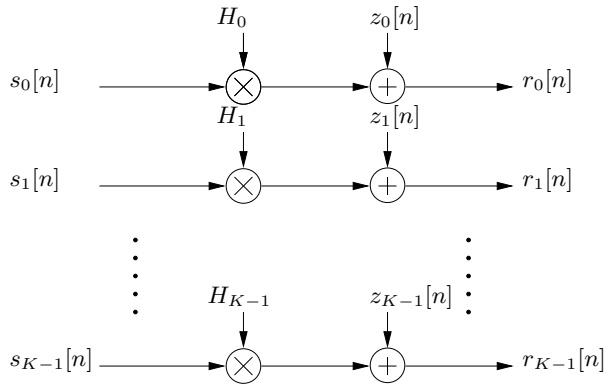

Figure 4.2: *Multiplicative input-output relation of the channel, as it is seen at the output of demodulator (FFT).*

OFDM systems are potentially able to mitigate ISI introduced by the channel as long as the cyclic prefix length is greater than the length of the channel impulse response. Moreover, the cyclically extended guard interval turns linear convolution of the signal and the channel into circular convolution. As a result, the frequency-selective channel is converted to a number of parallel flat channels; therefore a traditional complex time-domain equalizer can be replaced by a simple single tap frequency-domain equalizer. More precisely, we wish to obtain estimates of the K complex-valued channel coefficients gains on the parallel narrowband subcarriers.

Henceforth, we assume that the use of a cyclic prefix both preserves the orthogonality of the tones and eliminates intersymbol interference between consecutive OFDM symbols. Under these assumptions we can describe the system as a set of parallel Gaussian channels, shown in Figure 4.2. Thus, the received signal on the k^{th} subcarrier at time n is given by

$$r_k[n] = H_k s_k[n] + z_k[n]. \tag{4.2}$$

The most straightforward principle of channel estimation is to extract coefficients from received symbols by using transmit symbols, which are uniquely defined at the transmitter and are know at the receiver. The Least Squares (LS) estimate of the channel coefficient on k^{th} subcarrier $\hat{H}_k[n]$, given the received sample $r_k[n]$ and the known transmitted sample $s_k[n]$ can be calculated with

$$\hat{H}_k[n] = \frac{r_k[n]}{s_k[n]} = H_k[n] + \frac{z_k[n]}{s_k[n]}, \tag{4.3}$$

where $H_k[n]$ denotes the true channel coefficients and $z_k[n]/s_k[n]$ is residual noise. Thus without using any knowledge of the statistics of the channel, the LS estimates are calcu-

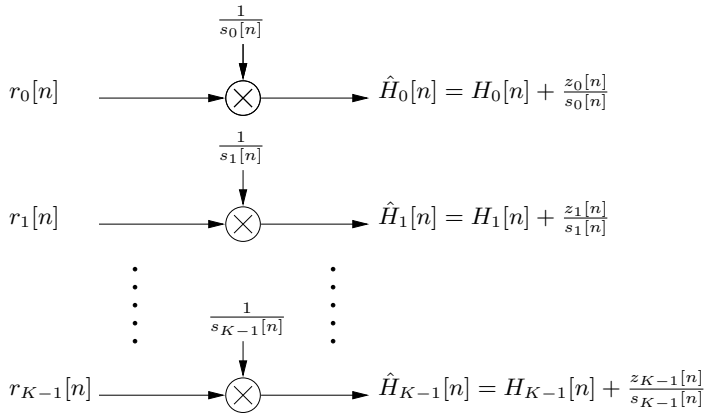

Figure 4.3: *Block diagram for LS channel estimation.*

lated by simple division as shown in Figure 4.3. The main drawback of this low complexity approach is high mean-square error.

Channel estimation can be performed based either on the short or on the long training symbols. However, it is quite intuitive that only non-zero pilot subcarriers can be used for channel estimation, since division by zero-valued $s_k[n]$ leads to some practical and implementation problems. Recall, that the short OFDM training symbol consists of 12 non-zero subcarriers, meaning that we could estimate at most one fourth of required channel coefficients. For this reason channel estimation in the developed model is based on the long training sequence.

LS channel estimation can be used as basis for more sophisticated techniques. One of such techniques implemented in the developed model is the so-called *averaged LS estimation* [11]. We first recall, that the standard defines two long training symbols. Taking advantage of this preamble structure we independently calculate LS estimates for the first $\hat{H}_k[1]$ and the second $\hat{H}_k[2]$ training symbol in accordance with Equation 4.3. The final channel estimate for the k^{th} subcarrier used for subsequent OFDM data symbols is the average of these two estimates:

$$\hat{H}_k = \frac{1}{2}(\hat{H}_k[1] + \hat{H}_k[2]). \tag{4.4}$$

Note, that this approach is only suitable for slow fading channels, such as block-fading. The fast fading channel causes complete loss of estimated channel parameters.

Other efficient channel estimation approach implemented in the developed model is based on the fact that the channel impulse response is short compared with the OFDM symbol length in any well-designed system. This specific structure of OFDM allows for so-called low-rank approximation [21], also known as *smoothing*. It can be shown that most of the energy of the channel impulse response observed after sampling in frequency-domain is con-

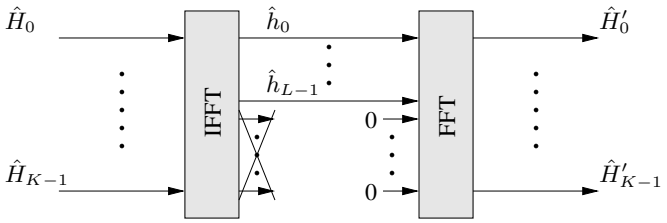

Figure 4.4: *Low-rank estimator structure.*

tained in, or near, the first L taps, where L denotes channel delay spread. In other words, the energy of the channel coefficients decreases rapidly outside the first L taps, whilst the noise energy is assumed to be constant over the entire range. In order to improve the performance of the LS estimator in terms of mean-square error for a range of SNRs we consider only the taps with significant energy and the elements corresponding to low energy taps are approximated by zero. This modification is illustrated in Figure 4.4.

4.3 Equalizer

We have already seen in Chapter 3 that the wireless channel can exhibit delay dispersion, which leads to ISI and disturbs the signal transmission. To reduce or eliminate ISI, the receiver uses an equalizer that simply reverses distortions introduced by the channel.

We still assume that the channel DS is not larger than the length of cyclic prefix, implying that the orthogonality of individual subcarriers is preserved and multiplicative input-output relation of the channel (see Equation 4.2) holds. Furthermore, at this point we assume perfect Channel State Information (CSI), i.e., all channel coefficients H_k are known at the receiver. Then the most straightforward approach to mitigate the influence of the channel is to use an equalizer with coefficients that are inverse-proportional to the channel coefficients, i.e., $E_k = 1/H_k$. This simple design strategy, that attempts to remove all of the ISI is known as Zero-Forcing (ZF) strategy. The equalization process is illustrated in Figure 4.5 and can be written in the discrete-time domain as

$$\hat{r}_k[n] = E_k r_k[n] = \frac{1}{H_k}(H_k s_k[n] + z_k[n]) = \frac{H_k s_k[n]}{H_k} + \frac{z_k[n]}{H_k} = s_k[n] + \tilde{z_k}[n]. \qquad (4.5)$$

Hence, the output of the equalizer is given by the plain transmitted sample $s_k[n]$ plus a noise component $\tilde{z}_k[n]$. However, the great disadvantage of ZF equalizer is its effect on the noise. At all time instances n where the channel coefficients H_k attain small values, the equalizer has a strong amplification, and thus also amplifies the noise.

Equation 4.5 demonstrates that the ZF structure perfectly equalizes the channel impulse

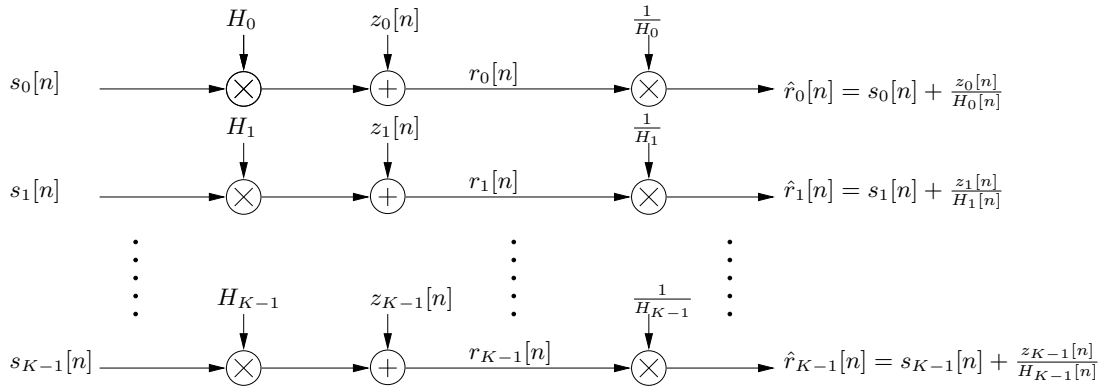

Figure 4.5: *OFDM system with equalizer.*

response and in fact it can even be shown [22] that the ML detector for pure OFDM systems is just the ZF equalizer followed by a threshold detector (hard demapping). In wireless communications, however, the channel is unknown and time-variant. The former problem can be solved by means of the channel estimator, as described in Section 4.2. Then the equalization process is based on estimated channel coefficients $\hat{H}_k$ instead of know coefficients H_k. Time variance implies that the channel coefficients $H_k[n]$ varies over time and thus the estimates used for equalization have to be adopted to the channel state at sufficiently short regular intervals. Since in the developed model channel estimation is based on long training symbols, channel coefficients are estimated just once, and then reused for the length of one frame. In Chapter 5 we will see that the model performs definitely poorer in time-variant channels as compared to block-fading channel, due to strong variation of channel coefficients, that can not be sufficiently precise estimated by just using the preamble.

4.4 Demapper and Decoder

4.4.1 Demapper

The samples at the output of the equalizer, which can be any complex numbers are first converted into a "detected" symbols $\hat{a}$ that are taken from the symbol alphabet $\mathcal{A} = \left\{a^{(1)}, a^{(2)}, \ldots a^{(M_a)}\right\}$. Certainly it is desirable that the detected symbols are equal to the symbols that were transmitted. However, it might happen that $\hat{a} \neq a$, meaning that a symbol error occurred.

In the next step each detected symbol $\hat{a}$ is demapped into the corresponding binary word, thereby inverting the bits $\rightarrow$ symbol mapping performed by the receiver (see Section 2.3.4). This results in a higher rate (remember that $R_b = lR_s$) detected coded bit sequence $\hat{c}_j$. If no symbol errors occurred, each detected coded bit equals the original. In presence of symbol

errors some of the detected coded bits will be incorrect, which does not necessary imply that the detected data bits $\hat{u}$ are incorrect as well. This is true since coded bit are protected by a channel code and thus detection errors, or at least some of them, can still be corrected.

The process of detection, i.e., mapping of sampled complex-values at the output of equalizer to valid symbols can be as simple as hard demapping, or more sophisticated as soft demapping. *Hard demapping* is based on the minimum Euclidian distance between the received symbols and all the valid symbols of the certain constellation. That is, the detected symbol $\hat{a}[n]$ is chosen as the valid symbol $a \in \mathcal{A}$ which, in the complex plane, has smallest Euclidian distance to the sampled output of equalizer [13]:

$$\hat{a}[n] = \arg\min_{a \in \mathcal{A}} |r[n] - a| = \arg\min_{a \in \mathcal{A}} \sqrt{(r_I[n] - a_I)^2 + (r_Q[n] - a_Q)^2}. \tag{4.6}$$

However, in order to decrease the probability of residual decoding errors it is advantageous to use *soft demapping* instead of hard. In contrast to hard demapping, soft demapping also reveal the reliability associated to the respective observation. Soft demapper observes the random complex values $r = r_I + jr_Q$ at the output of equalizer and bases its decision on the A-Posteriori Probability (APP) $Pc_i = 0|r$, which is a proper measure of the reliability information about the code bit c_i. Often, it is more convenient to work with Log-Likelihood Ratios (LLRs) instead of bit probabilities [23]. The a posteriori LLR of c_i, given the observation r, is defined as

$$\Lambda(c_i|r) = \log\frac{P(c_i = 1|r)}{P(c_i = 0|r)}. \tag{4.7}$$

The sign of $\Lambda(c_i|r)$ contains the information about the value of the bit $c_i \in 0, 1$. The magnitude of the LLR expresses the reliability of the associated decision. A large (small) value $|\Lambda c_i|$ corresponds to more (less) certainty about the value of the bit c_i.

Both hard and soft decision methods are implemented in the developed physical layer model and can be user-defined in the simulation settings block.

4.4.2 Deinterleaver

Hard or soft coded bits from the output of the demapper are fed into the deinterleaver block, which arranged the interleaved data back into the original sequence. As a result of this procedure, correlated noise introduced in the transmission channel appears to be statistically independent at the receiver and thus allows better error correction. Inverse relation performed by the deinterleaver is defined in two permutations.

Let j denote the index of the original received bit before the first permutation and i the index after the first and before the second permutation. The first permutation is then defined

by the rule:

$$i = s \cdot \text{floor}(\frac{j}{s}) + j + (\text{floor}(\frac{16 \cdot j}{N_{CBPS}}))\text{mod}\,(s), \qquad j = 0, 1, \ldots N_{CBPS} - 1, \tag{4.8}$$

where s is parameter dependent on the number of coded bits per subcarrier N_{BPSC} and is defined in Equation 2.14. The second permutation is given

$$k = 16 \cdot i - (N_{CBPS} - 1)\text{floor}(\frac{16 \cdot i}{N_{CBPS}}), \qquad i = 0, 1, \ldots N_{CBPS} - 1, \tag{4.9}$$

here k denotes the bit index after the second permutation, just prior to the convolutional decoder.

4.4.3 Decoder

If signal was punctured at the transmitter in order to increase the coding rate, i.e., some of the encoded bits were omitted, receiver has to compensate for this process before actual decoding can take place. Since values of the omitted code bits are unknown and the only information available in this context is their position in received coded bit sequence, receiver inserts a dummy "zero" metric. The inserted zeros have no influence on the metric calculation of the succeeding Viterbi decoder.

The IEEE 802.11 standard [10] recommends the Viterbi algorithm for decoding. The goal of the algorithm is to find the sequence $\hat{\mathbf{s}}$ that was transmitted with the highest likelihood, if the sequence $\mathbf{r}$ was received

$$\hat{\mathbf{s}} = \max_{a} \Pr(\mathbf{r}|\mathbf{s}), \tag{4.10}$$

where maximization is done over all possible transmit sequences $\mathbf{s}$ [15] and is based on the trellis diagram representation. The Trellis diagram cascades all possible state transitions representing a number of successive code symbol intervals corresponding to the total duration of transmission. Let the state ψ_k be defined as the current content of the shift register, representing convolutional encoder shown in Figure 2.8 at time k. When we pass from a time point k to the next time point $k+1$, the current referece data bit $u[k]$ enters the convolutional encoder from the left side, the oldest data bit leaves the shift register on the right side and all other data bits, contained in the shift register are shifted to the right by one position [13]. Evidently, the resulting new state ψ_{k+1} depends on the current state ψ_k and on the current data bit $u[k]$. Since for convolutional encoder with Rate $1/2$ each coded symbol is given as combination of $l = 2$ bits, there are $M_a = 2^l = 4$ possible states $\psi_k \in \{(0,0),(0,1),(1,0),(1,1)\}$ for each time instanse k. Different states ψ_k for some time index $k = 1, 2, \ldots$ are represented

by nodes of the trellis diagram and state transitions are given by the branches.[1] Each path through the entire length of trellis describes a certain sequence of states ψ_k, corresponding to the sequence of input data bits $\mathbf{u}$ and sequence of output code bits $\mathbf{c}$. In particular, if we know the path we know the corresponding input data bits. The Viterbi algorithm can be then defined as follows:

1. At each time k the k^{th} branch metric is calculated as the squared Euclidian distance $d_i^2[k] = |r[k] - s_i[k]|^2$ in the signal space diagram[2].

2. The current partial path metric, that is given as the sum of all individual branch metrics $d_i^2[k] = \sum_{l=1}^{k} |r[l] - s_i[l]|^2$ is recursively calculated.

3. From all partial paths running into a given node at time k, only the partial path with the smallest $d_i^2[k]$ is retained. Thus, at each stage of the trellis we eliminate the least likely paths.

4. This process of calculating the branch metrics, updating the partial path metrics, and discarting all partial paths except the survivors is repeated until we have used up all received code bits $r[k]$.

5. Finally, the optimum path is the survivor path with the smallest total path metric d_i^2.

Since only at the end of the trellis the total path metrics are known and thus the ML path can be determined, we have to wait until the end of the transmission before one can output even the first symbol. It is impractical in general and therefore, we force at the time k the decision on the data bit $\hat{u}[k-m]$ lying m symbol intervals back. Here m is a fixed integer called truncation depth and is in practice about five times the constraint length of the code.

It is important to note, that the Viterbi decoder can be used for hard or soft decoding, depending on decision type applied for demapping (see Section 4.4.1). If received symbols undergo hard decision before being fed to the decoder, the Viterbi decoder computes the Hamming distance between received symbols and possible symbols as a metric. In this case algorithm still exploits the fact that not all combination of bits are valid codewords, but does not use the knowledge about reliability of received bits. Performance of decoder can be improved considerably if we use soft information instead. In particular, this implies that the bits located close to the decision boundary have less impact on the finally chosen sequence than the bits that are far away from the boundary. Carefully note that by setting the decision

[1] Note, that not all pairs of successive states are connected by branches, which expresses the fact that not all state transitions are possible.

[2] Here, $r[k]$ is the received sequence of coded bits up to time index k, and $s_i[k]$ are all possible transmitted sequence

type in simulation settings block to hard or soft you immediately enforce both demapper and decoder to use the same decision type.

Finally decoded data bits $\hat{u}$ are descrambled with the same scrambler as used at the transmitter (see Section 2.3.1).

4.5 Error ratio calculation

Regardless of the receiver settings and channel characteristics, the Error Ratio (ER) provides the ultimate measure of performance for all digital communication systems, and for the developed model particularly. Critical dependencies of the model behavior on simulation settings will be presented in form of ER vs. SNR curves in Chapter 5. Therefore it is important to note, how this relations are calculated and which user-defined parameters are of particular importance for this calculations.

The model defines two measures of error ratio:

- The first is the Bit Error Rate (BER) calculation, that compares the transmitted bits $u[k]$ with demodulated and decoded bits $\hat{u}[k]$ outputted by the receiver. It calculates the BER as a running statistic, by dividing the total number of unequal pairs of data bits by the total number of input bits. If no SNR range is set, BER will be continuously calculated until simulation is manually terminated. By setting the SNR range it is important to define the number of bit pairs that will be compared for each SNR value. It is recommended to simulate over $10^6 - 10^7$ bits for each SNR, in order to average over sufficiently large number of channel realizations.

- For some applications, as i.e., comparison with results of real measurements, BER dependence cannot be seen as a sufficient measure of model performance. This is true, as in all real applications a frame is transmitted, passed over the channel and detected as whole, which is clearly different from bit-by-bit detection. Specifically it implies that the whole frame is considered as wrong, if just a single bit in frame was incorrectly detected. Thus for calculation of FER we still perform bitwise comparison of transmitted and detected bits, with the only difference that there are two counters. The inner counter computes the BER for each frame and passes the value of wrong bits to the outer counter. As soon as at least one bit is wrong the model assumes that the whole frame was detected wrong and increments the total number of frame errors. The outer counter then calculates the FER, by dividing the total number of unsuccessfully detected frames by the total number of transmitted frames.

In the past three chapters we have discussed in detail the theoretical background, design, and the most important implementation aspects of the developed model. The ER calculation block concludes this discussion and brings us to the discussion of simulation results, where we will see how certain model parameters and simulation settings influence the overall model performance.

5

Simulation Results and Comparison to Real Measurements

In this chapter the model performance with different transceiver structures and in various propagation environments is evaluated. First several simulation results for transmission over the AWGN channel are compared with analytical BER vs. SNR curves in order to verify accurate functioning of the simulator. Further we underline the system dependence on certain parameters of the propagation environment, e.g., number of multipath components, frequency of channel time-variations, relative speed of vehicles, etc. Throughout this section we demonstrate in a comparative manner possible combinations of user-defined parameters that strictly determine the performance of the physical layer, in order to get a complete overview of the simulator features and deeper feeling of the transmission mechanisms. Finally FER performance results for time-variant channel are compared with results from real-world measurements, certain similarities are observed and possible reasons for differences are discussed.

5.1 Performance in AWGN

As already stated in Chapter 3 the AWGN channel is not a typical propagation model for vehicular networks, however it is implemented in the developed model mainly as a reference for validation of system's consistency and stability. It is well known that for uncoded transmission over a simple AWGN channel with QAM constellation and Gray mapping, BER performance curves can be calculated based on pairwise conditional probabilities. The probability of an error is simply the probability of the transmitted symbol being shifted in the constellation diagram beyond a certain threshold, so that the received symbol and the transmitted symbol are not equal anymore. The error probability for antipodal one-dimensional signals like BPSK can be found in any digital communication textbook, i.e., in [14] and is given as:

$$P_b = Q(\sqrt{\frac{2E_b}{N_0}}), \tag{5.1}$$

here the Q-function defined as $Q(x) = 1/\sqrt{2\pi}\int_{\infty}^{x} e^{-\xi^2/2}d\xi$ is the probability that a Gaussian random variable X with zero-mean and variance 1 is larger than x, i.e., $Q(x) = P\{X > x\}$ and E_b/N_0 is the SNR per bit. The same Equation 5.1 can be used for the bit error probability calculation of QPSK signals, which is due to the fact that QPSK is basically the same antipodal signal that in contrast to BPSK is two-dimensional and thus spectral efficiency is increased without decreasing minimum distance between symbols.

However closed-form expression of the bit error probability, as given in Equation 5.1 can only be found for such simple constellations as BPSK and QPSK, where the decision regions are half-planes. Of course, an exact evaluation of bit error probability for M-ary QAM can be obtainable for arbitrary M as well, however it is tedious to express the result in a closed form. Derivation of approximations for bit error probability of 16 QAM and 64 QAM constellations is very intuitive but quite lengthy and for this reason will be skipped here (detailed derivation can be found in [24], [25] or [26]). Final closed-form approximations of bit error probabilities for 16 QAM and 64 QAM are given in Equation 5.2 and 5.3, respectively.

The bit error probability for the 16 QAM modulation scheme is approximated as:

$$\begin{aligned} P_b &= \frac{1}{2}\sum_{k=1}^{2} P_b(k), \qquad \text{with} \\ P_b(1) &= \frac{1}{4}\left[\operatorname{erfc}(\sqrt{\frac{2E_b}{5N_0}}) + \operatorname{erfc}(3\sqrt{\frac{2E_b}{5N_0}})\right] \textit{and} \\ P_b(2) &= \frac{1}{4}\left[2\operatorname{erfc}(\sqrt{\frac{2E_b}{5N_0}}) + \operatorname{erfc}(3\sqrt{\frac{2E_b}{5N_0}}) - \operatorname{erfc}(5\sqrt{\frac{2E_b}{5N_0}})\right]. \end{aligned} \tag{5.2}$$

The bit error probability for 64 QAM signal is approximated as:

$$
\begin{aligned}
P_b &= \frac{1}{3}\sum_{k=1}^{3} P_b(k), \qquad \text{with} \qquad (5.3)\\
P_b(1) &= \frac{1}{8}\left[\operatorname{erfc}(\sqrt{\frac{E_b}{7N_0}}) + \operatorname{erfc}(3\sqrt{\frac{E_b}{7N_0}}) + \operatorname{erfc}(5\sqrt{\frac{E_b}{7N_0}}) + \operatorname{erfc}(7\sqrt{\frac{E_b}{7N_0}})\right];\\
P_b(2) &= \frac{1}{8}[\ 2\operatorname{erfc}(\sqrt{\frac{E_b}{7N_0}}) + 2\operatorname{erfc}(3\sqrt{\frac{E_b}{7N_0}}) + \operatorname{erfc}(5\sqrt{\frac{E_b}{7N_0}}) + \operatorname{erfc}(7\sqrt{\frac{E_b}{7N_0}})\\
&\quad - \operatorname{erfc}(9\sqrt{\frac{E_b}{7N_0}}) - \operatorname{erfc}(11\sqrt{\frac{E_b}{7N_0}})\Big];\\
P_b(3) &= \frac{1}{8}[4\ \operatorname{erfc}(\sqrt{\frac{E_b}{7N_0}}) + 3\operatorname{erfc}(3\sqrt{\frac{E_b}{7N_0}}) - 3\operatorname{erfc}(5\sqrt{\frac{E_b}{7N_0}}) - 2\operatorname{erfc}(7\sqrt{\frac{E_b}{7N_0}})\\
&\quad + 2\operatorname{erfc}(9\sqrt{\frac{E_b}{7N_0}}) + \operatorname{erfc}(11\sqrt{\frac{E_b}{7N_0}}) - \operatorname{erfc}(13\sqrt{\frac{E_b}{7N_0}})\Big].
\end{aligned}
$$

In both equations the function erfc$(\cdot)$, given as $\operatorname{erfc}(x) = 2/\pi \int_x^\infty \exp(-u^2)du$ is the complimentary error function.

In Figure 5.1 the simulated BER performance for uncoded transmission with BPSK, QPSK, 16QAM and 64 QAM is compared with theoretical approximations (dashed lines), given in Equations 5.1, 5.2 and 5.3. From completely overlap of the analytical curves with simulation results we can conclude that:

1. the subcarrier SNR definition mentioned in Chapter 3 is accurate, since there are no shifts between analytical and simulated curves;

2. the overall model performance with uncoded transmission is verified, since it matches the theoretical expectations.

Next in Figure 5.2 we compare BER performance of coded transmission over AWGN channel for all available combinations of modulation schemes and coding rates, listed in Table 2.1. The BER vs. SNR performance of 16 QAM and 64 QAM is significantly poorer than that of BPSK and QPSK. This is mainly because for a given SNR value, the symbols of 16 QAM and 64 QAM constellations have to be more densely spaced than the symbols of the BPSK and QPSK constellations, which immediately implies higher error probabilities. This is the price paid for larger spectral efficiency of 16 QAM and 64 QAM. Furthermore it is important to note that the punctured codes (i.e., codes with coding rate $3/4$ and $2/3$) require a higher SNR to achieve the same BER performance as for unpunctured codes of equal constellation, due to the reduced redundancy of the code and thus decreased error correction capability of decoder.

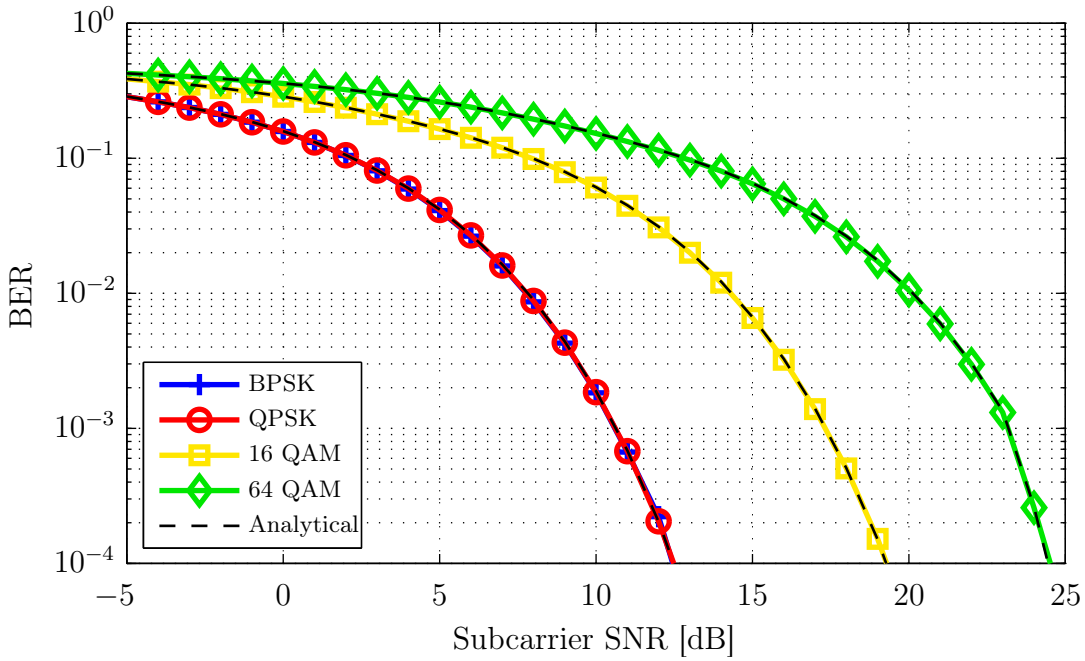

Figure 5.1: *Simulation results of uncoded transmission over the AWGN channel compared with BER curves analytically derived in Equations 5.1, 5.2 and 5.3.*

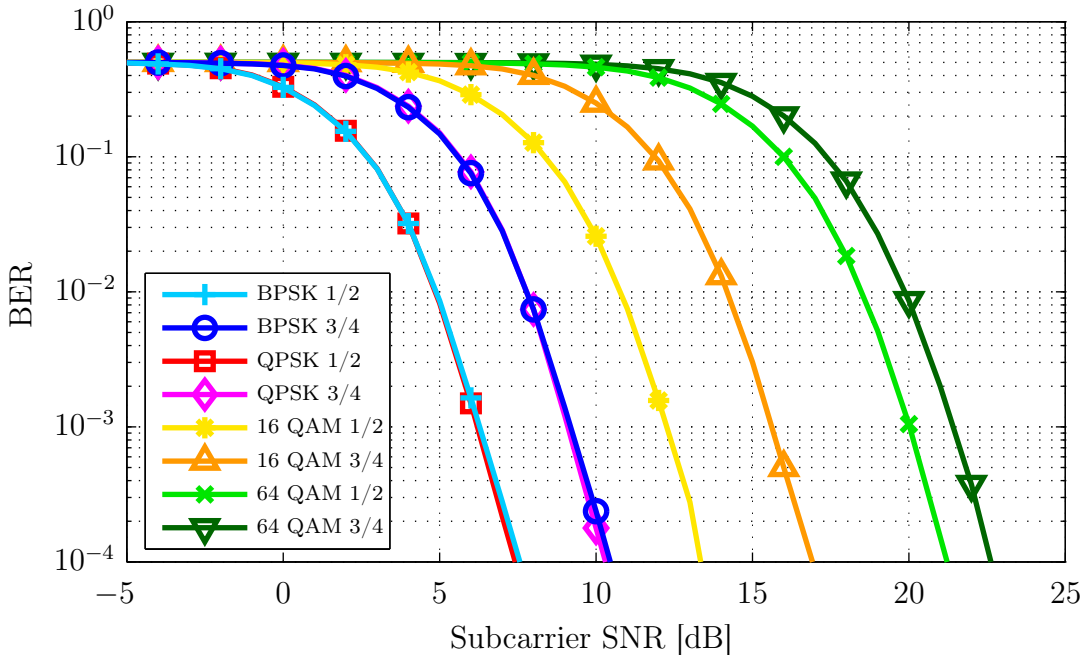

Figure 5.2: *Comparison between simulation results of different modulation schemes and coding rates for coded transmission over an AWGN channel.*

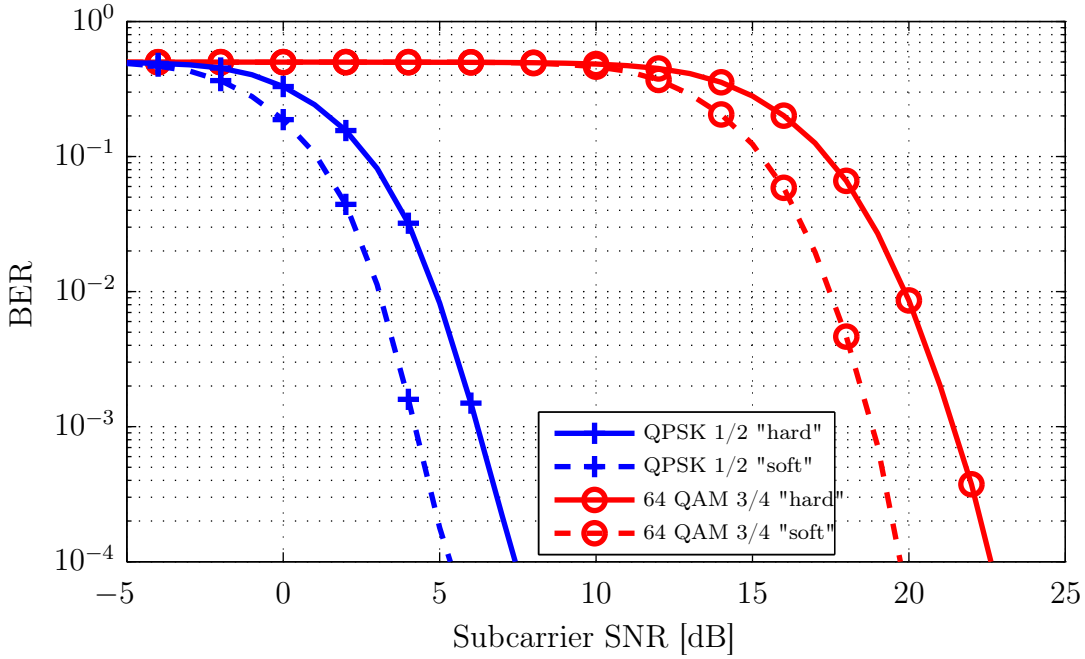

Figure 5.3: *Effect of using soft information on overall model performance for coded transmission over AWGN channel.*

Further user-defined parameter for the AWGN channel is the demapping and the decoding type that can be chosen between hard and soft. The effect of using soft information in the receiver on the performance of the entire link is shown in Figure 5.3 for QPSK with rate $1/2$ and 64 QAM with rate $3/4$. For both modulation schemes, as well as for all other, performance gain of about 2 dB can be achieved at higher SNR values when soft demapping and decoding structure is used.

5.2 Performance in Block-Fading Channels

This section investigates physical layer performance in propagation environments with block-fading. Transceiver structure for this channel model allows for uncoded and coded transmission in combination with hard or soft demapping and decoding at the receiver, similarly as for the AWGN channel. In the previous section we have shown that coded transmission and the use of soft information significantly increases the model performance, which is true for block-fading channels as well. While channel coding is implemented in most, if not all, practical realizations, processing of the soft information increases complexity of the receiver and thus is not always applied. Therefore, if nothing else is stated in this section we assume coded transmission over block-fading channel with hard demapping and decoding.

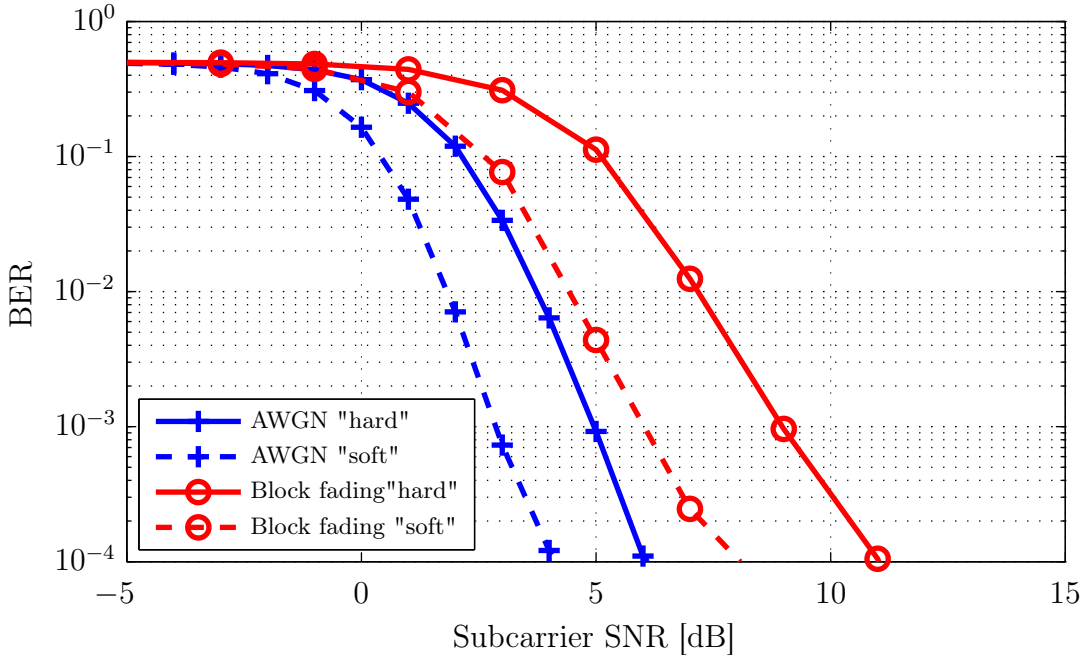

Figure 5.4: *Comparison of the BER vs. SNR performance achievable with soft and hard demapping and decoding schemes for AWGN and block-fading channels. Results are obtained for coded QPSK transmission with rate* $1/2$*. For the block-fading channel we assume perfect CSI and ZF equalization at the receiver, DSL* = 15*, RMSDS* = 4*.*

Figure 5.4 on one hand compares the BER vs. SNR model performance in an AWGN channel with that from a block-fading channel and on the other hand we indicate the significant gain that can be achieved if soft information is used at the receiver. Results for the block-fading channel assumes perfect CSI and the use of ZF equalizer. Although the channel impulse response is shorter than the length of the cyclic prefix and the channel coefficients are known, it is not possible to compensate the frequency-selective fading effects introduced by the channel. As already mentioned in Chapter 3 the multipath propagation environment induces multiple copies of the transmitted signal that create either constructive or destructive interference at the receiver. In particular, very small channel coefficients enhance significantly the noise component of the received signal, therefore loss in BER performance of about 3-4 dB as compared to the AWGN channel is obtained.

The general conclusion that by increasing the number of elements in a symbol alphabet, we can achieve higher data rates at the cost of the deteriorated BER performance holds for a block-fading channel as well, as is illustrated in Figure 5.5. Side-by-side comparison of Figures 5.2 and 5.5 yields following observations:

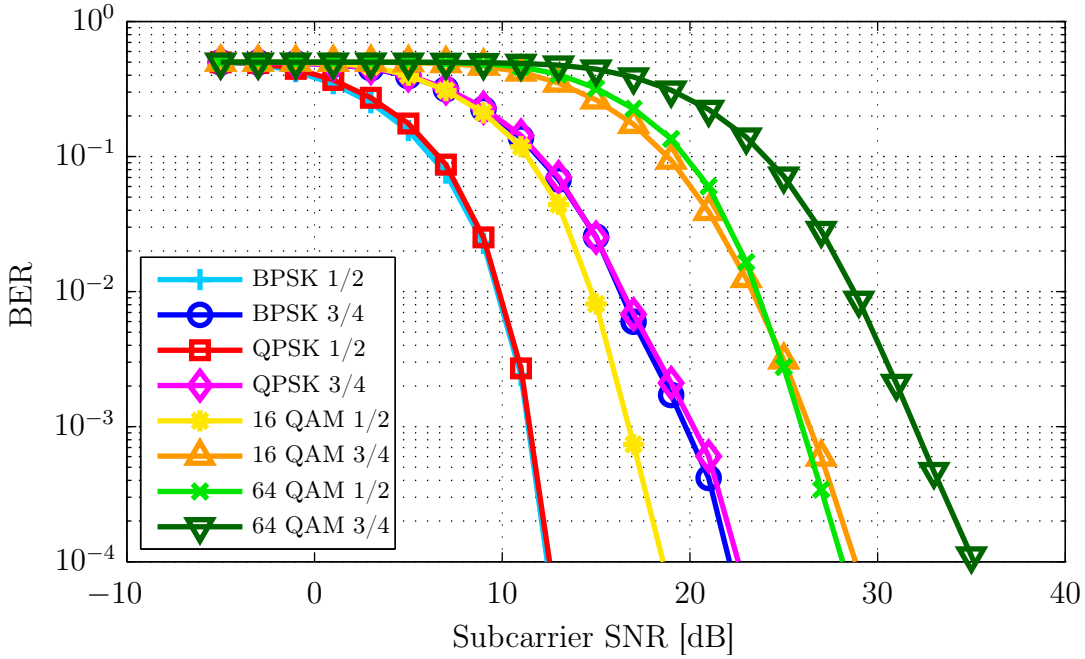

Figure 5.5: *Comparison between simulation results of different modulation schemes and coding rates for coded transmission over a block-fading channel.*

- BPSK and QPSK curves still fall together, meaning that with the same BER performance QPSK allows for doubling the data rate
- Punctured codes (i.e., codes with coding rate $3/4$ and $2/3$) transmitted over a block-fading channel show much poorer BER performance, as compared with the AWGN channel, indicating higher demand on error correction capability of the code. For instance, punctured BPSK and QPSK codes perform worse than unpunctured 16 QAM, specially at the higher SNR values. Thus one can conclude that for transmission over fading channels in order to achieve a higher data rate it is more advantageous to increase the number of symbols in the symbol alphabet and thus place constellation points closer to each other, rather than reduce redundancy and thus error correction capability of the code.
- The best BER performance is still achievable with unpunctured BPSK and QPSK codes, it seems a reasonable compromise between data rate and BER to consider QPSK with coding rate $1/2$ as standard modulation and coding combination for further discussions and comparison in the rest of this chapter.

Recall that the block-fading channel introduces frequency-selectivity due to multipath propagation and that the channel coefficients remain constant within one frame. In Sec-

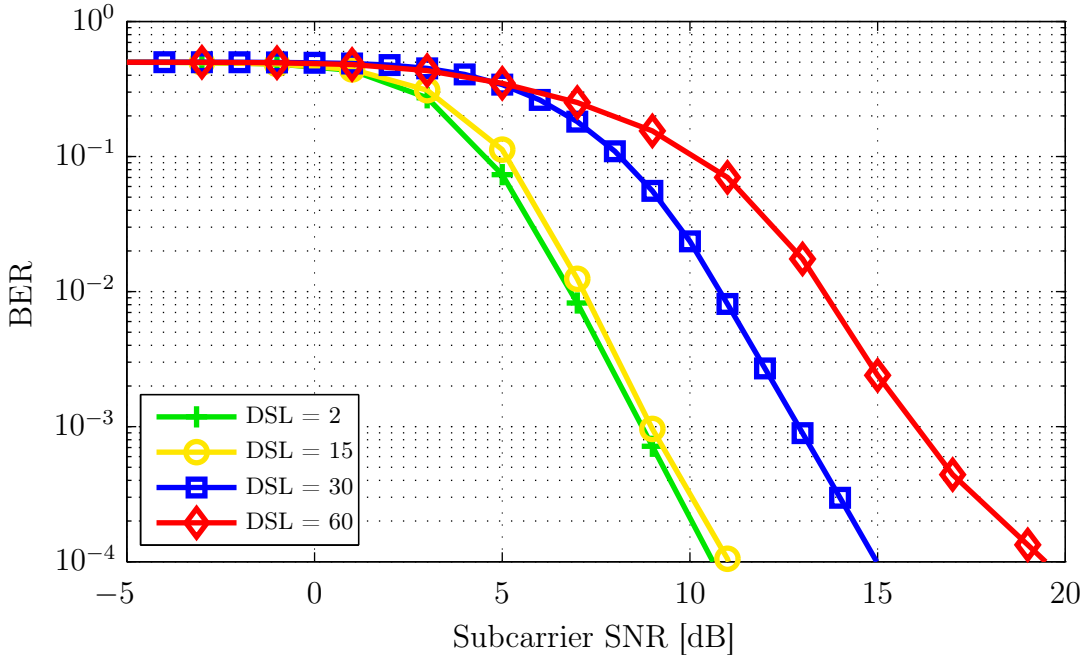

Figure 5.6: *Simulation results for unpunctured coded QPSK transmission over block-fading channel with various DSLs. We assume perfect CSI, ZF equalization and constant RMSDS = 4 for all iterations.*

tion 2.1 we have shown that if the Delay Spread Length (DSL) of the channel is shorter than the length of the cyclic prefix (16 samples in this implementation), the frequency-selective fading channel can be converted to a number of parallel flat-fading channels, yielding a simple multiplicative input-output channel relation and complete discarding of ISI. Figure 5.6 indicates influence of channel's DSL on overall model performance undergoing block-fading. The BER performance curve for a channel with just single delayed replica in addition to first arrived component (DSL = 2) is just insignificantly better than that of a channel with DSL = 15, meaning that the effect of multipath propagation is nearly negligible if DSL is shorter, or in marginal case equals the cyclic prefix length. If the channel DSL is longer than the cyclic prefix length, i.e., DSL = 30 or DSL = 60 (blue and red curves in Figure 5.6, respectively) the receiver is not able to disregard effects of ISI; as result a loss of 4 dB to 7 dB in the BER performance as compared to channels with DSL shorter than the cyclic prefix is obtained. In order to compensate for multipath propagation effects introduced by the channels with long DSL, some OFDM transmission schemes introduce a length-adaptive cyclic prefix [27], however this improvement comes at the cost of the reduced data rate.

5.3 Performance in Time-Variant Channels

This section examines model dependence on various parameters of time-variant channel. Parameters representing effects of multipath propagation are, as in case of block-fading channel, DSL and RMSDS; their distortive impact on the overall model performance remains the same and thus will not be explicitly analyzed in this section. Other than the merely frequency-selective fading channel, this channel model introduces dependence on relative speed of vehicles that significantly affect the overall model performance and will be evaluated later on. A further important outcome of the time-variant fading channel being fast varying, in contrast to slow-fading described in the previous section, is that model performance is conditioned on the number of OFDM data symbols in each transmitted frame.

Figure 5.7 demonstrates the model performance with various modulation parameters propagating via time-variant channel. All simulation results in this figure assumes perfect CSI, ZF equalization, vehicle speed of 80 km/h, DSL = 15 and RMSDS = 4. Comparing these results with BER vs. SNR relations plotted for the same modulation and coding parameters in case of a block-fading channel we can conclude that the curves are slightly shifted to the right, due to Inter Carrier Interference (ICI) introduced by the Doppler spread. However, this relation between block-fading and time-variant channel models holds as long, as we assume perfect CSI information and thus all channel coefficients are known and the effect of the channel up to ICI can be disregarded by the equalizer.

As soon as the channel coefficients have to be estimated, what is definitely the case in all practical implementations, the model experiences dramatic degradation in the BER performance. Figure 5.8 illustrates the change in the BER vs. SNR performance of the coded QPSK transmission over the time-variant channel with relative speed of 80 km/h, DSL = 15 and RMSDS = 4, introduced by using LS estimates for equalization, instead of known channel coefficients. The reason for this degradation is the fast fading nature of the channel, which on one hand implies that the channel coefficients estimated based on the preamble are not sufficiently precise for equalization of the residual OFDM symbols in a frame. On the other hand time-variations within one OFDM symbol introduce ICI, which appears to be one of the most critical impairing factors to the performance of an OFDM based V2V communication system. ICI is a main reason for the high error floor observed in Figure 5.8, this particularly implies that for arbitrary large SNR value this propagation scenario does not allow for BER higher than $3 \cdot 10^{-3}$.

The above mentioned effect of imperfect channel estimation is presented in Figure 5.9. Due to the fast fading nature LS estimates based on the long training sequence, as described in Section 4.2 do not match actual channel coefficients of the subsequently data OFDM symbols. This dismatch of channel coefficients and their estimates grows with each symbol, and thus

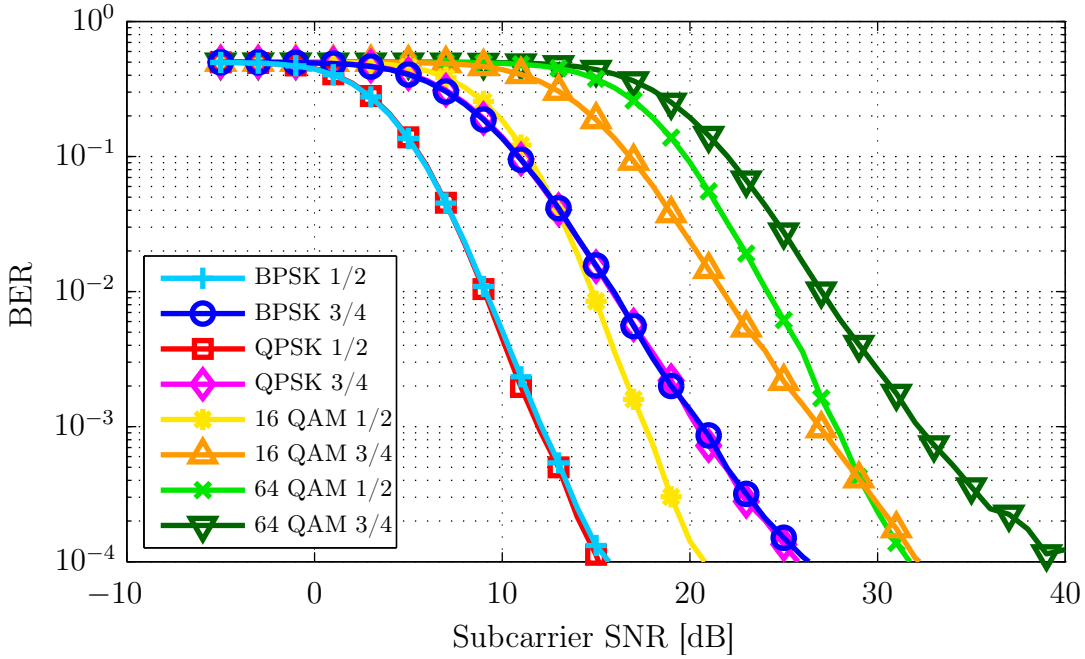

Figure 5.7: *Comparison between simulation results of different modulation schemes and coding rates. Relative velocity* 80 *km/h, DSL* = 15*, RMSDS* = 4*. Receiver assumes perfect CSI and ZF equalization.*

while for short frame length (up to 5 OFDM data symbols) acceptable BER performance can be achieved with simple LS estimator, for longer frames, i.e., 260 OFDM data symbols per frame model performance deteriorates enormously and we obtain an error floor already at $2 \cdot 10^{-1}$. In other words, even with arbitrary high SNR value approximately 20 % of all bits will be detected wrong, which is unacceptable in terms of FER performance, which is more important for practical implementations. One feasible solution for this problem is to make the frame length short enough, so that the LS estimates based on the preamble can still sufficiently compensate the effect of the channel in payload. This however, will reduce the throughput of the system. Another option would be to implement more sophisticated channel estimation techniques.

Additional to the frame length, crucial for model performance in a fast-fading environment is the Doppler spread introduced by fast motion in the wireless link. Figure 5.10 demonstrates impairing effect of relative velocity between the transmitter and the receiver on the overall model performance. For low velocities about 30 km/h and relatively short frame length (Figure 5.10 assumes 15 OFDM symbols per frame) it is even possible to achieve a constant error floor around 10^{-4}. However, Doppler spread and thus ICI increases proportionally to the relative velocity and for vehicle speed of 200 km/h it is not possible to achieve

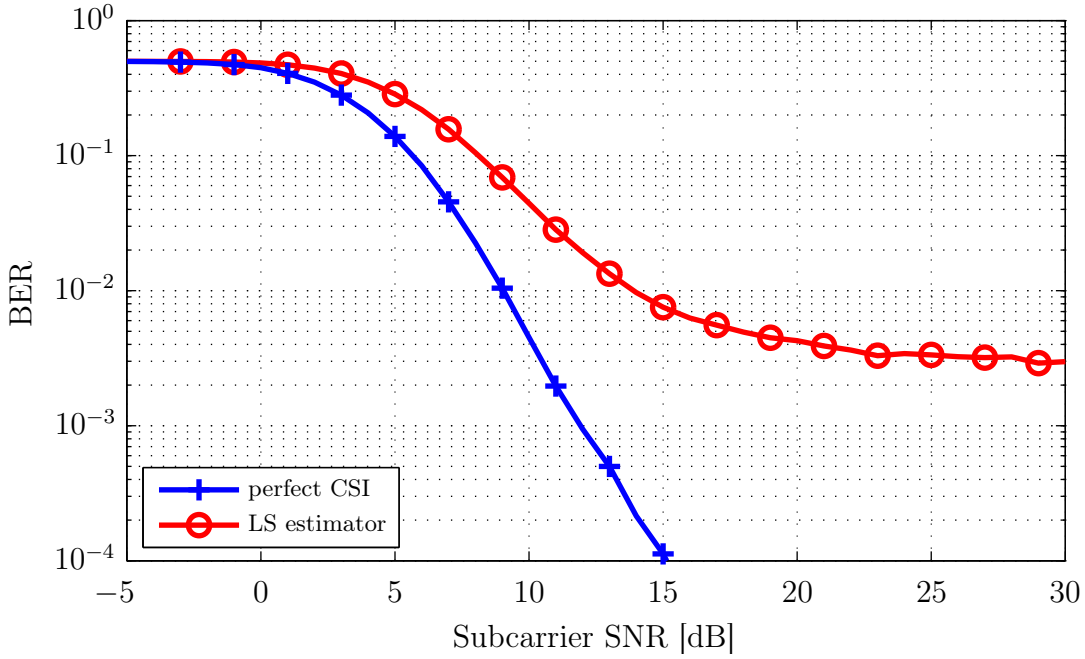

Figure 5.8: *Comparison of model performance in a time-variant channel, where known channel coefficients or LS estimates are used for signal equalization at the receiver.*

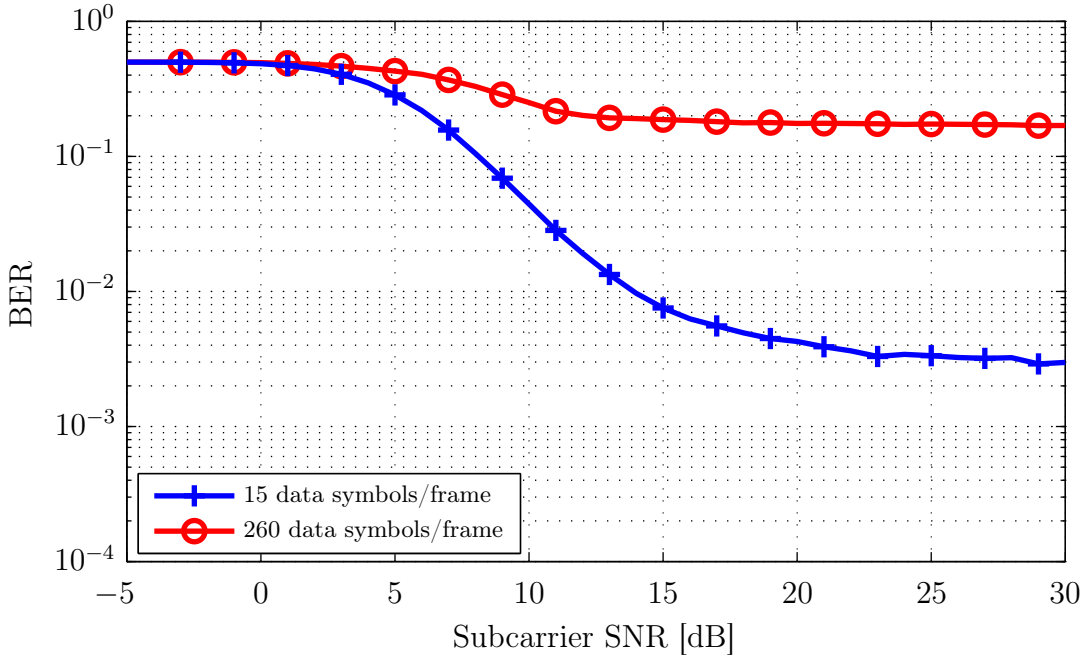

Figure 5.9: *LS estimator performance shown in terms of BER vs. SNR relation for 15 and 260 OFDM data symbols in each frame.*

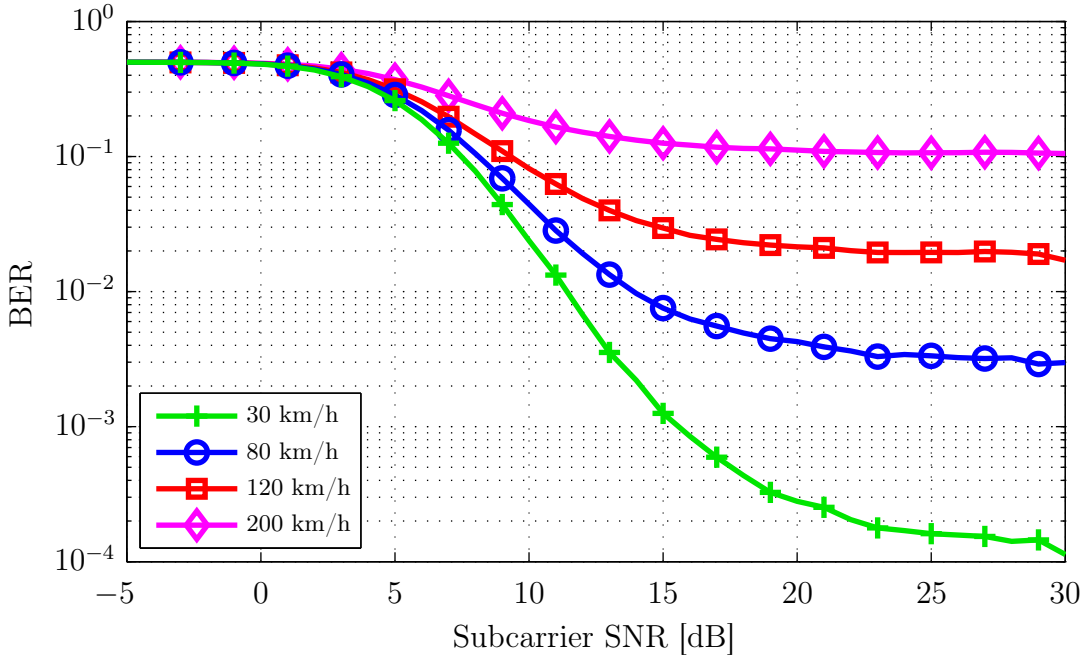

Figure 5.10: *The BER performance dependence on relative vehicle velocity. All curves are plotted for coded unpunctured QPSK transmission with* 15 *OFDM data symbols per frame over a time-variant channel with DSL* = 15*, RMSDS* = 4*. Receiver performs ZF equalization based on LS channel estimates.*

the BER performance better than 10^{-1} even for the most robust modulation and coding combination (QPSK with rate 1/2) and short frame length.

In Section 3.3 we have introduced two channel models for vehicular test environments with PDP other than exponential that was always considered up to now. Recall that the Vehicular A ITU channel model has a relative delay of 2510 ns which is then smoothed with sinc interpolator over 30 samples, therefore the channel impulse response is longer than the cyclic prefix length. However, with perfect CSI it is still possible to achieve the BER performance just slightly worse compared to those of the time-variant channel with exponential PDP of DSL shorter than the length of cyclic prefix. If the channel coefficients are unknown and have to be estimated, the physical layer model experiences a performance decrease of approximately 10 times, i.e., the error floor of time-variant channel with DSL = 15 is obtained at about $3 \cdot 10^{-3}$, while for the Vehicular A channel model already at $5 \cdot 10^{-2}$, as shown in Figure 5.11. This is definitely the effect of ISI that comes along to ICI introduced by Doppler spread, due to the motion in wireless links. The Vehicular B ITU channel model has a relative delay of 20000 ns, meaning that delay spread by far exceeds length of cyclic prefix, furthermore from Figure 3.2b we can conclude that the delay copies of the k^{th} subcarrier of n^{th} OFDM symbol are spread by the channel not only over consecutive $n + 1^{\text{th}}$ symbols, but

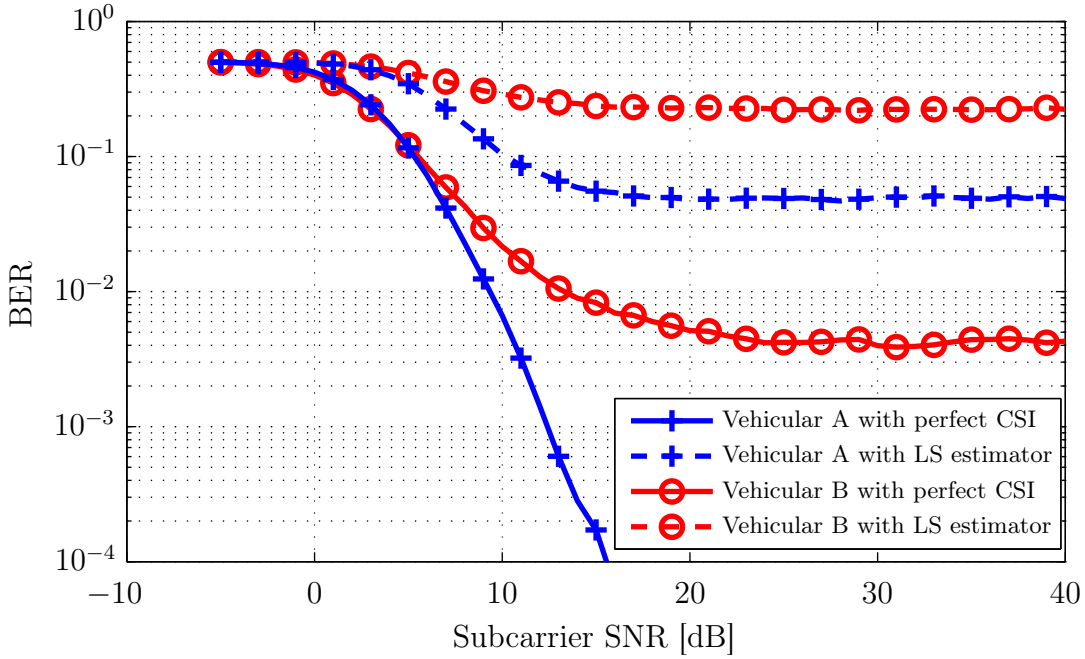

Figure 5.11: *Model performance in vehicular A and vehicular B channels, where either known channel coefficients or LS estimates are used for signal equalization at the receiver. Curves are plotted for coded unpunctured QPSK transmission with* 15 *OFDM data symbols per frame over time-variant channel with PDP defined in Table 3.1 and vehicle velocity of* 80 *km/h.*

even over the $n + 2^{\text{th}}$, causing very strong ISI. Thus such a PDP definition results in both ICI and very distinct ISI that the receiver with arbitrary long cyclic prefix is not able to combat. As consequence thereof simulation results show relatively high error floor of about $4 \cdot 10^{-3}$ even with perfect CSI at the receiver that, as we have seen, was not the case either for the time variant channel with DSL = 15 or for the vehicular A channel. Of course in absence of CSI the BER performance of the model is even further impaired and we obtain an error floor at about $2 \cdot 10^{-1}$; nearly the same BER performance was achieved in absence of ISI for the time-variant channel with very high relative velocity of 200 km/h, as shown in Figure 5.10.

To conclude this section Figure 5.12 presents side-by-side comparison of the physical layer model performance in various propagation environments. All curves are plotted for coded unpunctured QPSK transmission with 15 OFDM data symbols per frame. Multipath components of block-fading channel and time-variant channel are given with DSL = 15 and RMSDS = 4. Time-variant channels assume a vehicle velocity of 80 km/h. The receiver performs ZF equalization based on LS channel estimates.

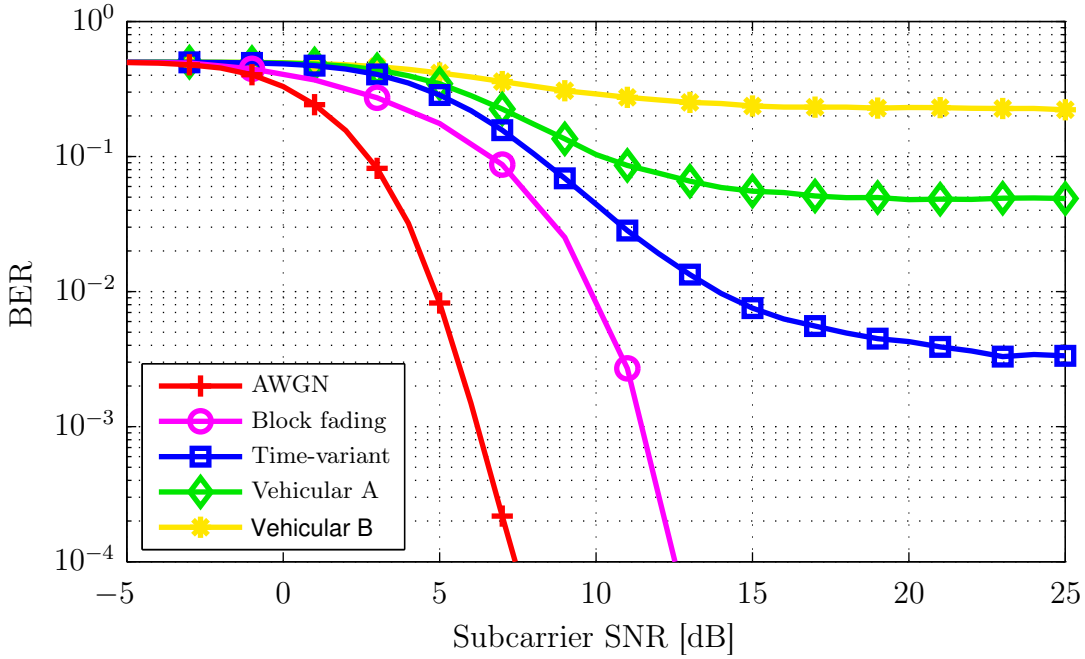

Figure 5.12: *Side-by-side comparison of system performance with all available channel models.*

5.4 Comparison to Real-World Measurements

As already mentioned in Section 4.5 BER vs. SNR relation is the ultimate measure of performance for all digital communication systems, however in most of the practical applications it is either too tedious or even not possible at all, to compare transmitted and received sequences in a bit-wise manner. Most of the practical implementations, including those based on the standard IEEE 802.11, append the checksum to the end of the payload for the purpose of detecting accidental errors that may have been introduced during its transmission over the channel. After detection and decoding the receiver calculates the checksum for the received message and compares it with the received checksum, appended by the transmitter. If the two checksums are not equal the whole received frame is considered as wrong and has to be retransmitted; this particularly implies that a single wrong bit in the frame results in a wrong frame.

WAVE performance real-world measurements for I2V communications have been carried out in July 2009 in Tyrol, Austria, along the highway A12, within the national Austrian project Real-time Safety-related Traffic Telematics (REALSAFE) [28]. In this measurements campaign the dependence of system performance on the following parameters were investigated:

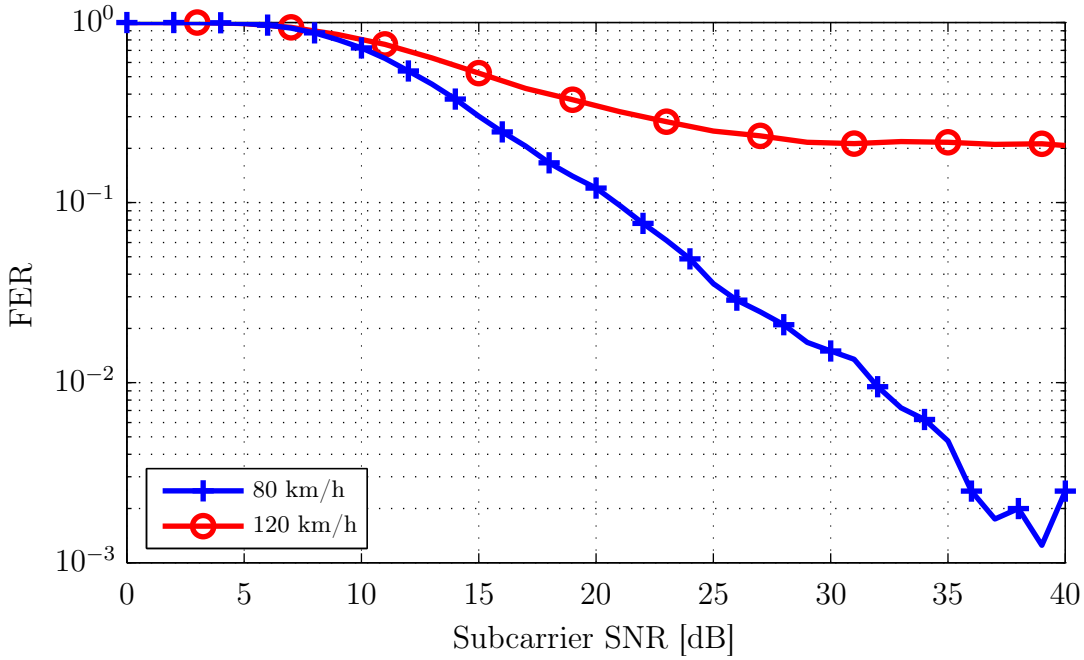

Figure 5.13: *The FER performance dependence on relative vehicle velocity. All curves are plotted for coded unpunctured BPSK transmission with* 14 *OFDM data symbols per frame over time-variant channel with DSL* = 15*, RMSDS* = 4*.*

- data rate (combination of certain symbol constellation and coding rate)
- frame length (number of OFDM data symbols per frame)
- vehicle speed

Results of the measurements were analyzed and summarized in sufficient detail in [29]. In order to compare the FER performance of developed model with the outcomes of the measurements, numerous simulations were performed over 1000 frames for each SNR value. The propagation environment was simulated based on time-variant channel model with exponentially decaying PDP with DSL = 15, RMSDS = 4 and two different vehicle speeds: 80 km/h and 120 km/h. The receiver was assumed to perform hard demapping and decoding, LS estimation with smoothing and ZF equalization.

Figure 5.13 compares the model performance for two different vehicle speeds: 80 km/h and 120 km/h, both for coded unpunctured BPSK transmission of the frame, containing 14 OFDM data symbols over the time-variant channel. As it was shown in Figure 5.10 for the BER performance, the Doppler spread introduced by the high relative motion between the transmitter and the receiver causes strong signal degradation due to ICI and thus characteristic bit error floor was obtained at approximately $3 \cdot 10^{-3}$ and $2 \cdot 10^{-2}$ for vehicle speed of 80 km/h

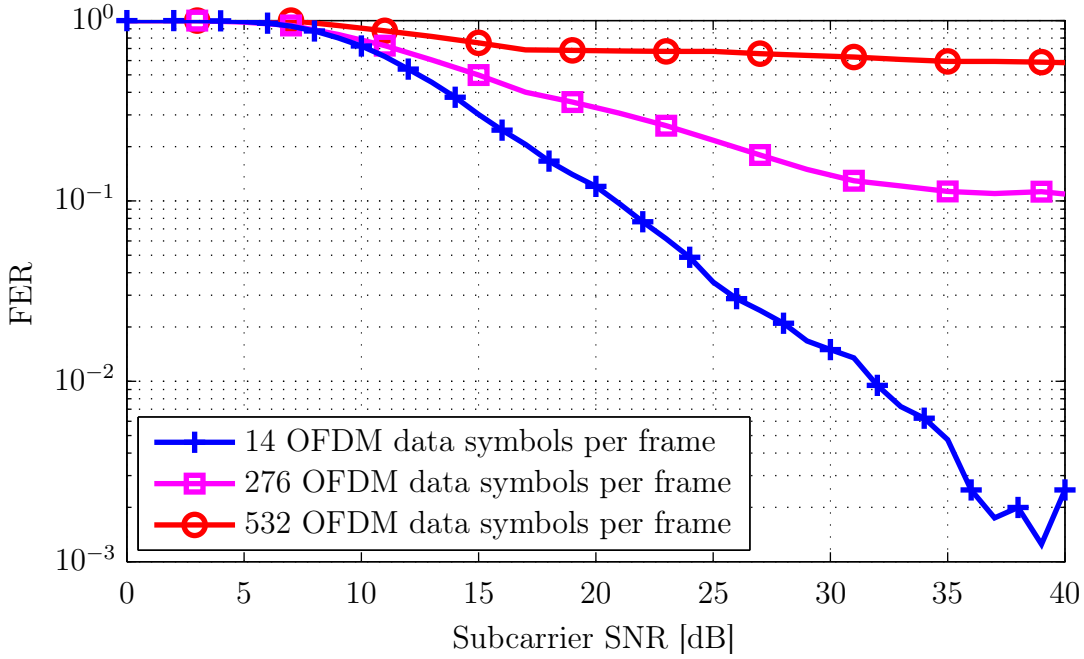

Figure 5.14: *The FER performance dependence on the packet length. All curves are plotted for coded unpunctured BPSK transmission over the time-variant channel with DSL = 15, RMSDS = 4 and vehicle velocity of 80 km/h.*

and 120 km/h, respectively. Thus the results obtained in Figure 5.13 are quite intuitive:

- For the vehicle speed of 80 km/h we obtain a constant decrease of the FER for the SNR values between 10 dB and 35 dB; whereas already at 21 dB the acceptable FER threshold [29] of 10^{-1} is achieved and for the SNR values starting with 35 dB the FER vs. SNR curve saturates and only few frame errors occur.

- For a vehicle speed of 80 km/h the distinct error floor at about $2 \cdot 10^{-1}$ emerges for SNR values starting with 30 dB. Thus even for such a short frame length (14 OFDM data symbols), where channel equalization with LS estimates performs almost as good as with perfect CSI, approximately $1/5$ of all transmitted frames are corrupted, due to strong ICI.

Comparing this results with the results presented in Table 5.2 of [29], one can conclude that in order for simulation platform to achieve the sufficient FER threshold of 10^{-1} for the vehicle speed of 80 km/h the SNR of 10 dB more is required, as compared to the results of the measurements. Whereas for vehicle speed of 120 km/h this threshold is not achievable at all.

In Figure 5.14 we compare the FER performance of the simulator for 3 different frame

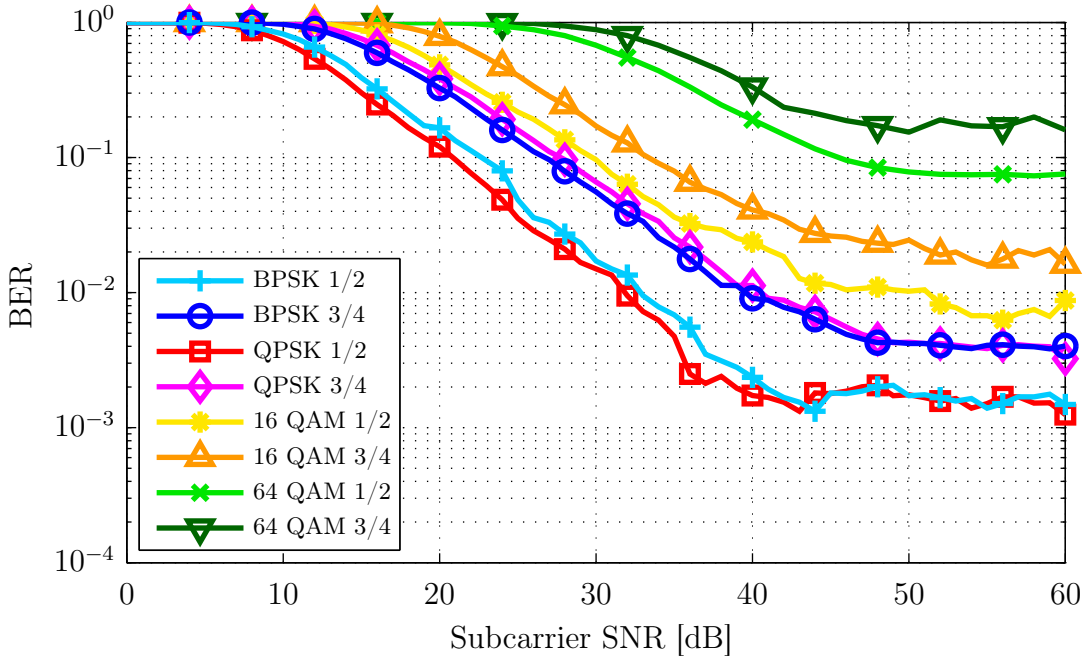

Figure 5.15: *The FER performance with different modulation schemes and coding rates. All curves are plotted for coded transmission over time-variant channel with DSL = 15, RMSDS = 4 and vehicle velocity 80 km/h. Each frame contains 14 OFDM data symbols. Receiver performs ZF equalization based on LS channel estimates.*

length: 0 byte, 787 byte and 1554 byte, corresponding to 14, 276 and 532 OFDM data frames [10], respectively, if BPSK with rate $1/2$ is used. The vehicle speed for all simulations is assumed to be 80 km/h. As mentioned above with the frame length of 0 byte, and thus nearly perfect channel estimation it is possible to achieve the FER threshold of 10^{-1} with SNR of about 21 dB. With packet length of 787 bytes and thus 276 OFDM data symbols per frame the desirable threshold is achieved with SNR of at least 33 dB, which is around 20 dB more, as compared to measurements results in Table 5.2 of [29]. With packet length of 1554 bytes the 10^{-1} threshold is not achievable and for arbitrary high SNR starting with 17 dB about 60 % of all received frames are wrong.

Figure 5.15 demonstrates model performance with various modulation parameters propagating via time-variant channel with vehicle speed of 80 km/h, DSL = 15 and RMSDS = 4. Each frame contains 14 OFDM data symbols and the receiver still performs ZF equalization based on LS estimates of channel coefficients. The model performance can be compared with results of measurements with equal settings, summarized in Table 5.3 of [29]. The threshold FER value of 10^{-1} is achievable with modulation schemes and coding rates except for 64 QAM with rate $3/4$, with which FER vs. SNR curve saturates at about $2 \cdot 10^{-1}$. The curves

shows a similar behavior to the BER vs. SNR curves, i.e., we obtain characteristic shift to the right when number of symbols in the symbol alphabet or coding rate is increased.

Comparing the simulation results with results of the real-world measurements presented in [29], we conclude that while the general FER progress with growing SNR is quite similar, the relation between FER and SNR is not the same and the simulated FER performance is at least 10 dB poorer. Potential reasons for this mismatch are:

- Another way of the SNR definition
- Offset in the SNR estimation (see [29] for more detailed explanation)
- Enhanced structure of the receiver used for the measurements
- Channel model used in simulation does not sufficiently precise reproduces the actual channel statistics.

6

Conclusions

Vehicular communications are turning to reality, driven by navigation safety requirements and by the investments of car manufacturers and public transport authorities. Their opportunities and areas of applications are growing rapidly and include many kinds of services with different goals and requirements. However, to bring its potency to fruition, vehicular networks have to cope with some challenging characteristics, which include potentially large scale and high mobility. Consequently, inter-vehicle communication is attracting a considerable attention from the research community and the automotive industry. This thesis starts by introducing the main applications and services supplied by vehicular communications as well as the underlying technologies, and standards. Further on, it provides a detailed overview of the physical layer components, interconnections and structures, as they are defined in the draft amendment IEEE 802.11p and investigates system performance in various propagation scenarios based on a physical layer model built with Matlab SIMULINK.

The developed simulator is based on OFDM system with 64 subcarriers and is absolutely consistent with the standard. In Chapter 2 of this thesis a detailed overview of the OFDM symbol and the transmit frame structure was given. While the symbol structure is strictly defined in the standard, the model allows some freedom by the definition of the transmit frame structure or at least of its length. Later on we have analyzed the dependence of model performance on the number of OFDM data symbols in one frame and tried to define acceptable upper bound of the frame length. It turned out to be quite a challenging compromise between short frame length needed for successful channel estimation in fast varying propagation environment and longer frame length required for higher throughput. Further parameter that specifies the operation mode of transmitter and has considerable impact on the overall system performance is the combination of symbol alphabet and coding rate. It was shown

that regardless of the channel model, the modulation schemes with lower coding rate and less densely spaced symbols of the signal constellation allow for significantly better BER performance.

Physical layer efficiency was extensively evaluated in realistic mobile communication channel conditions, ranging from pure AWGN channel to doubly-selective fading channel. Since the AWGN channel model constitutes to propagation environments without any fading effects, i.e., when there exists only one propagation path and there is no relative movement between transmitter and receiver, it is not a typical scenario for vehicular communications. However, this channel model was implemented in order to verify transceiver functionality. The AWGN channel BER performance, presented in Section 5.1, is evidence that the developed physical layer model is capable of precisely reproducing the analytical results of uncoded and coded transmission in non-fading, pure AWGN channel conditions. The influence of realistic multipath fading channel effects on the overall transmission performance was investigated with the block fading channel model that can be seen as a slow frequency-selective channel. To obtain realistic outdoor frequency-selective channel conditions an exponentially decaying PDP with Rayleigh distributed amplitude of channel coefficients was proposed, whereas the length of PDP or, equivalently, relative delay spread and RMSDS are user-defined parameters. In Section 5.2 we have evaluated the model performance in multipath propagation scenarios with various relative delay spreads and concluded that the effects of ISI on the transmission error statistics are negligible as long as the delay spread is shorter than the cyclic prefix. Besides the multipath propagation vehicular communications are typically characterized by the velocity of relative motion between the transmitter and the receiver that results in carrier frequency shift of each multipath component, due to the Doppler effect. The impact of time-varying Doppler shift was modeled with the Jake's spectrum, which is induced on each multipath component. In Section 5.3 we have shown simulation results for time-variant channel with various frame lengths, vehicle velocities, PDP and lengths of the delay spread. The most straightforward conclusion of the simulation results is that ICI caused by time-variations within one OFDM symbol, imposes lower limit on BER that cannot be exceeded even with arbitrarily high SNR.

The receiver introduced in Chapter 4 performs the preamble-based LS estimation and ZF equalization in order to invert distortive effect of the channel. By means of simulation results we compare the model performance in slow and fast fading channels, when either perfect CSI is assumed or LS estimates are calculated, for further signal equalization. For slow fading channels, like the block-fading model, simple preamble-based LS estimates averaged over two long training symbols are sufficiently precise for successful equalization of the rest of the frame, and thus model performance is just insignificantly different from the one, where perfect CSI is assumed. This, however, is not the case in fast time-varying propagation envi-

ronments that cause complete loss of the estimated channel parameters and introduce strong dependence on the frame length. Further consideration regarding the receiver structure is the use of soft information, between demapper and decoder that contains not only the hard bit, but also the degree of bit reliability given by the approximate LLRs. Typical asymptotic gains, ranging from 1.5 dB to 3 dB, were observed for hard decision over soft decision demapping and decoding algorithms.

This study touched a broad variety of fields within digital communications, ranging from transceiver design and channel modeling to implementation aspects of simulation platform. Accordingly, several prospective research areas were identified and are listed below:

- First and foremost it is clear that channel estimation and equalization remain extremely important issues for receiver design. While numerous studies and research activities have shown that the simple combination of ZF equalizer and LS estimator is an optimum compromise between receiver complexity and overall model performance for OFDM systems, we have obtained a relatively high error floor, when signal was propagating over a time-variant channel. Therefore implementation of more sophisticated estimation techniques, i.e., pilot-based channel estimation, seems to be an important subject for further model development.

- Although the implemented fading channel models, presented in Sections 3.2 and 3.3 are capable of adequately reproducing the statistical nature of real life fading channels they are just simplified empirical models and hence can barely be used for comparison of simulation results with results of real-world measurements. Thus, definition and modeling of real-world V2V or V2I scenarios with simulation tools like WinProp turns to be reasonable model extension.

- Further, the almost intuitive model extension would be applying multiple antennas at both ends of a communication system. The use of multiple antennas at both transmitter and receiver provides a diversity advantage that means a significant increase in capacity, i.e., higher data rates are achieved without increasing neither the bandwidth nor the total transmission power and greatly improvement of the BER vs. SNR performance.

- The last, but not the least important possible model extension is the implementation of the adaptive modulation and coding technique that is designed to track the channel variations and to adjust the transmitted power level, the symbol rate, the coding scheme, the constellation size, or any combination of these parameters to the link quality, improving the spectrum efficiency of the system, and reaching, in this way, the capacity limits of the underlying wireless channel.

List of Acronyms

AWGN Additive White Gaussian Noise

APP A-Posteriori Probability

BER Bit Error Rate

CCA Cooperative Collision Avoidance

CEPT European Conference of Postal and Telecommunications Administrations

CSI Channel State Information

DS Delay Spread

DSL Delay Spread Length

ER Error Ratio

ETSI European Telecommunications Standards Institute

EWM Emergency Warning Message

FDMA Frequency Division Multiple Access

FER Frame Error Ratio

FFT Fast Fourier Transformation

FIR Finite-length Impulse Response

GI Guard Interval

ICI Inter Carrier Interference

IFFT Inverse Fast Fourier Transformation

ISI Inter Symbol Interference

ISM Industrial, Scientific and Medical

ITS Intelligent Transport Systems

I2V Infrastructure-to-Vehicle

LOS Line-of-Sight

LLC Logical Link Control

LLRs Log-Likelihood Ratios

LS Least Squares

LTI Linear Time Invariant

LTV Linear Time Variant

MAC Medium Access Control

NLOS Non-Line-of-Sight

OFDM Orthogonal Frequency Division Multiplexing

OSI Open Systems Interconnection

PDF Probability Density Function

PDP Power-Delay Profile

PARP Peak-to-Average Power Ratio

PHY Physical Layer

PLCP Physical Layer Convergence Protocol

PMD Physical Medium Dependent

PSDU PLCP Service Data Unit

PPDU PLCP Protocol Data Unit

REALSAFE Real-time Safety-related Traffic Telematics

RMSDS Root Mean Square Delay Spread

SNR Signal-to-Noise-Ratio

S/P Serial-to-Parallel

TCP Transmission Control Protocol

UDP User Datagram Protocol

V2I Vehicle-to-Infrastructure

V2V Vehicle-to-Vehicle

WAVE Wireless Access in Vehicular Environments

WSMP WAVE Short Messages Protocol

ZF Zero-Forcing

Bibliography

[1] Y. Z. Hassnaa Moustafa, *Vehicular Networks Techniques, Standards and Applications*. Taylor & Francis Group, LCC, 2009.

[2] F. S. Biswas, R.Tatchikou, "Vehicle-to-vehicle wireless communication protocols for enhancing highway traffic safety," *IEEE Communication Magazine*, vol. 44, pp. 74 – 82, 2006.

[3] "Commision decision on the harmonised use of radio spectrum in the 5875-5905 MHz frequency band for safety-related applications of intelligent transport systems (ITS)." 2008/671/EC, August 2008.

[4] CEPT, "CEPT report 20." Report from CEPT to EC in response to the Mandate on the harmonised radio spectrum use for safety critical applications of Intelligent Transport Systems (ITS) in the European Union, December 2007.

[5] ETSI, "Intelligent transport systems (ITS); radiocommunications equipment operating in the 5 855 MHz to 5 925 MHz frequency band; harmonized EN covering essential requirements of article 3.2 of the R&TTE directive." Draft ETSI EN 302 571 V0.0.2, December 2007.

[6] IEEE Intelligent Transportation Systems Committee, "Trial-use standard for wireless access in vehicular environments (WAVE) - resource manager." IEEE Std 1609.1-2006, 2006.

[7] IEEE Intelligent Transportation Systems Committee, "Trial-use standard for wireless access in vehicular environments (WAVE) - networking services." IEEE Std 1609.3, April 2007.

[8] IEEE Intelligent Transportation Systems Committee, "Trial-use standard for wireless access in vehicular environments (WAVE) - security services for applications and management messages." IEEE Std 1609.2-2006, 2006.

[9] IEEE 802.11p, "Draft standard for information technology - telecommunications and information exchange between systems - local and metropolitan area networks - specific requirements: Wireless access in vehicular environments." IEEE P802.11p/D9.0, September 2009.

[10] IEEE Computer Society, "IEEE standard for information technology - telecommunications and information exchange between systems - local and metropolitan area networks - specific requirements part 11: Wireless LAN medium access control and physical layer specifications." IEEE Std 802.11, June 2007.

[11] G. Matz, "Wireless OFDM systems." Lecture Notes, 2008.

[12] F. Hlawatsch, "Information theorie and coding." Lecture Notes, October 2008.

[13] F. Hlawatsch, "Modulation and detection technique." Lecture Notes, March 2009.

[14] J. G. Proakis, *Digital Communications*. 3rd ed., 1995.

[15] A. F. Molisch, ed., *Wireless Communications*. 2005.

[16] D. Morgan, "Analysis and realization of an exponentially-decaying impulse response model for frequency-selective fading channels," *Signal Processing Letters, IEEE*, vol. 15, pp. 441 – 444, 2008.

[17] S. Pätzold, "Methods for modeling of specified and measured multipath power-delay profiles," *IEEE Trans. Veh. Technol*, vol. 50, pp. 978–988, 2002.

[18] S. McEliece, "Channels with block interference," *Information Theory, IEEE Transactions*, vol. 30, pp. 44 – 53, 1984.

[19] Y. Zheng and C. Xiao, "Simulation models with correct statistical properties for Rayleigh fading channels," *IEEE Transactions on communications*, vol. 51, no. 6, pp. 920–928, 2003.

[20] I. Recommendation, "ITU-R Recommendation M. 1225," *Guidelines for evaluation of radio transmission technologies for IMT-2000*, 1997.

[21] J. Van de Beek, O. Edfors, M. Sandell, S. Wilson, and P. Borjesson, "On channel estimation in OFDM systems," in *1995 IEEE 45th Vehicular Technology Conference*, vol. 2, 1995.

[22] Z. Wang, X. Ma, and G. Giannakis, "Transactions Papers OFDM or Single-Carrier Block Transmissions?," *IEEE Transactions on Communications*, vol. 52, no. 3, 2004.

[23] J. Hagenauer, E. Offer, and L. Papke, "Iterative decoding of binary block and convolutional codes," *IEEE Transactions on Information Theory*, vol. 42, no. 2, pp. 429–445, 1996.

[24] D. Yoon, K. Cho, and J. Lee, "Bit error probability of M-ary quadrature amplitude modulation," vol. 5, 2000.

[25] M. Fitz and J. Seymour, "On the bit error probability of QAM modulation," *International Journal of Wireless Information Networks*, vol. 1, no. 2, pp. 131–139, 1994.

[26] L. Hanzo, S. Ng, T. Keller, and W. Webb, *Quadrature amplitude modulation*. John Wiley, 2004.

[27] Z. Zhang and L. Lai, "A novel OFDM transmission scheme with length-adaptive Cyclic Prefix," *Journal of Zhejiang University-Science A*, vol. 5, no. 11, pp. 1336–1342, 2004.

[28] "Overview of REALSAFE project." https://portal.ftw.at/projects/realsafe.

[29] D. Faetani, "IEEE 802.11p Physical Layer Performance Analysis of Infrastructure-to-Vehicle Real World Measurements," Master's thesis, Vienna University of Technology Institute of Communications and Radio-Frequency Engineering, 2010.